Doppler Radar Dual Polarization Considerations for NEXRAD

Part II

Dale Sirmans, Dusan S. Zrnic', N. Balakrishnan

National Severe Storms Laboratory
U.S. Department of Commerce
National Oceanic and Atmospheric Administration
1313 Halley Circle
Norman, Oklahoma

December 1988

Prepared for

Joint Systems Program Office
National Weather Service
National Oceanic and Atmospheric Administration
U.S. Department of Commerce
Rockville, Maryland

Doppler Radar Dual Polarization Considerations for NEXRAD - Part II

EXECUTIVE SUMMARY

The report addresses present state of polarimetric measurements and considers the technical aspects of the inclusion of such capability into the NEXRAD system. Polarimetric measurements can be included without compromising NEXRAD's prime mission, and at the scanning rates presently required to map weather hazards.

A sequence of alternately polarized horizontal and vertical fields is proposed because it is easily processed, the effects of propagation are separated, and the performance with the existing antenna is satisfactory.

It is shown that dual polarization measurements result in improved quantification of hydrometeors based on the following variables: 1) differential reflectivity defined as the ratio of reflectivities at orthogonal linear polarizations. The two reflectivities are a measure of drop dimension in the respective directions, and are different, if the hydrometeors are anisotropic and have a preferred orientation. 2) differential propagation constant defined as the range rate of change of the difference between the phases of horizontally and vertically polarized fields. It is a measure of liquid water along the propagtion path. 3) correlation coefficient between orthogonally polarized echoes. This parameter is sensitive to the distribution orientation and shape of hydrometeors. Significant system enhancements over single polarization measurements realized when the three parameters are combined are: Variance of rainfall rate is reduced, and at higher rain rates, the bias of the mean estimate is also lower; discrimination between rain and hall as well as other hydrometeors; potential to categorize hail size (further exploration is needed to quantify this capability).

The range resolution for polarimetric measurements is about 1 km. We have demonstrated, on actual time series data, the signal processing techniques required to retrieve both polarimetric and Doppler parameters. Theoretical processing errors have been computed and verified with weather data.

Engineering changes to accommodate dual polarization measurements are in 1) microwave circuitry, 2) signal processing, and 3) data analysis. In the microwave circuitry addition of dual linear polarization requires addition of a switch and an orthomode coupler. Signal processing requires hardware and software modifications to adapt the existing calculations to estimation of the three polarimetric measurables. Data analysis would entail software changes in order to incorporate the measurements into output products.

Addition of polarimetric capability into the NEXRAD system is not recommended at this time. We have established the operational potential of dual polarization and shown that the measurement is compatible with the prime mission of the radar. However, the utility and cost effectiveness of the technique, for operational agencies, have to be demonstrated. We recommend that an operational test system be configured and that a program be established to demonstrate the technique and provide data for evaluation.

Doppler Radar Dual Polarization
Considerations for NEXRAD
Part II

Doppler Radar Polarization Report
Considerations for NEXRAD

D. Sirmans, D.S. Zrnic', and N. Balakrishnan
National Severe Storms Laboratory
National Oceanic and Atmospheric Administation
Department of Commerce
1313 Halley circle
Norman, OK 73069

Introduction

The purpose of this report is to examine the present state of polarimetric measurements on weather radars. This is a follow-up of a previous NSSL report (Sirmans et al., 1984, revised 1986) and no repetition of previous material will be made. We also confine our literature survey to the years since 1985 and present only findings that may be pertinent to NEXRAD applications. Theory, measurements, and technology are analyzed.

During the last three years several groups here and abroad were involved in polarimetric measurements (Schnabl et al., 1986; Bringi et al., 1986; Illingworth et al., 1987; Mueller and Staggs, 1986; Sachidananda and Zrnic', 1987; Aydin et al., 1986; Goldhirsh et al., 1987). To be exact there are four radars with 10 cm wavelength which have obtained measurements and one with 5 cm wavelength. All four radars (10 cm wavelength) utilize switching between vertical and horizontal polarization. This type of polarimetry is simple yet effective and does not require a super low sidelobe antenna. Dual linear polarization is the method recommended for consideration by NEXRAD.

Until very recently the only two parameters measured were differential reflectivity and linear depolarization ratio. The differential reflectivity, Z_{DR}, is the ratio of reflectivity at horizontal polarization to the reflectivity at vertical polarization (Seliga and Bringi, 1976). The two reflectivities are different if hydrometeors are anisotropic. They are relatively

easily measured since it suffices to transmit with a horizontal polarization and then receive the strong echo. The same holds for vertical polarization. This measurement is favored and easy because the strong (co-polar) echo is dominant. Furthermore good estimates of rain rate and discrimination of hail is possible.

Linear depolarization ratio is the ratio of the orthogonal polarization component to the co-polar component. The measurement requires two receivers, one for the co-polar and the other for the orthogonal (cross-polar) component. In principle this measurement is straightforward but in practice it is difficult because the cross-polar component is often 20 to 30 dB below the co-polar and must compete with noises, echoes through sidelobes, etc. Linear depolarization ratio has not been nearly as useful as differential reflectivity. Linear depolarization ratio is not considered a viable measurement for NEXRAD.

Differential propagation phase constant, K_{DP}, is another parameter that Doppler radar can estimate, if it is capable of measuring Z_{DR}. This parameter was proposed by Seliga and Bringi (1978) but has been so far exploited only by Sachidananda and Zrnic' (1987), and Steinhorn and Zrnic' (1988). As a matter of fact, in the most efficient practical scheme to estimate Z_{DR} and Doppler parameters one must account for the differential phase ϕ_{DP} (Sachidananda and Zrnic', 1988). This breakthrough scheme (developed with JSPO support) makes polarization measurements possible on NEXRAD by reducing differential measurement dwell time to that compatible with the prime mission of the system. It is only a small step from ϕ_{DP} to K_{DP}; thus the differential propagation constant comes in essentially free. No hardware modifications are needed and the only added calculation is one subtraction per dwell time per range location and scaling! Of course if a field of K_{DP} values is to be displayed, provisions for such software and interpretation of data must be made.

The third parameter that we consider is the correlation coefficient between horizontally (H) and vertically (V) polarized echoes; $\rho_{HV}(o)$, that would be obtained if H and V were transmitted and received simultaneously. This parameter depends on the distribution of hydrometeor shapes, orientation and their rotational motions; it complements Z_{DR} and K_{DP}. However, because H and V are alternately transmitted, special care and assumptions must be made in order to retrieve $\rho_{HV}(o)$.

Each of the polarization measurables has advantages for diagnosing specific hydrometeor types. Differential reflectivity is a good hail indicator and can be used together with the reflectivity factor, Z, to quantify pure rain. Propagation phase constant, K_{DP}, has a unique property that allows discrimination between statistically isotropic and anisotropic scatterers (such as between hailstones and raindrops). It is only affected by the aligned scatterers, whereas differential reflectivity is affected by both. This is because on the average the phase shift of horizontally and vertically polarized electric fields after propagation through randomly oriented scatterers (such as hail) is the same, whereas waves propagating through aligned scatterers (such as rain) experience relatively large phase shifts.

The correlation between horizontal vertical waves, $\rho_{HV}(o)$, depends on the distribution of hydrometeor shapes, orientation and their rotational motions. Little physical modelling of $\rho_{HV}(o)$ is available; however, heuristic arguments suggest that this parameter could be used to gauge hail size.

Section 1 of this report discusses the meteorological quantification using the dual polarization technique. Section 2 discusses the gist of data processing that allows simultaneous Z_{DR} and K_{DP} calculations at rates commensurate with the prime mission of NEXRAD. Section 3 discusses the engineering required and the resulting system performance.

1. Quantification of hydrometeors with Dual Polarization

We briefly examine methods based on polarimetric measurements that may allow better discrimination of hydrometeor types and estimation of rain rate. It is worth noting that polarization variables are usually represented as data field in the radar coordinate system. Each field, by itself or in combination with others, may be used towards achievement of stated goals. As we shall shortly see the proposed methods are very simple; they do not require approaches based on artificial intelligence or expert systems but rely on thresholds or combination of thresholds for hydrometeor discrimination, and, equations for rain rate estimation.

1.1 Rainfall estimation

It is the belief of the authors that a well calibrated radar with continuous autocalibration checks, such as implemented on the NEXRAD, will be able to produce high quality estimates of rain rate most of the time. Some adjustment of the Z,R relationship may be needed and that can be accomplished with few rain gages. However, there are important instances when polarization measurement may produce information heretofore not available by other means. For example in the presence of hail Z,R relationships are not reliable and may grossly overestimate the amount of rainfall. Also, in theory polarimetric measurements of rain rate are less sensitive to the variation of the drop size distributions. We will examine briefly rain measurements.

A standard method using reflectivity alone is to invert the Marshall-Palmer drop size distribution and obtain rain rate as:

$$R(Z_H) = 0.0365 \cdot 10^{0.0625\, Z_H} \ (\text{mm h}^{-1}), \qquad (1.1)$$

where Z_H is the effective reflectivity factor for horizontally polarized waves in dBZ.

In the Z_{DR} method one needs to solve for two parameters of an exponential or gamma DSD after assuming a relationship between size and shape of raindrops. Then in pure rain the rainrate vs Z_H, Z_{DR} relationship has a form (Ulbrich and Atlas, 1984):

$$R(Z_H, Z_{DR}) = 1.93 \cdot 10^{-3} \cdot Z_{DR}^{-1.5} \; 10^{0.1 Z_H} \; (\text{mm h}^{-1}), \qquad (1.2)$$

where Z_H is in dBZ and Z_{DR} is in dB.

Finally, a relationship between K_{DP} and rain rate (Sachidananda and Zrnic' 1987) is:

$$R(K_{DP}) = 20.35 \; K_{DP}^{0.866} \; (\text{mm h}^{-1}), \qquad (1.3)$$

where K_{DP} is in deg km^{-1}.

This last method is the least sensitive of the three to the DSD variations. That is because the integrand that determines K_{DP} contains the drop diameter raised to the power of 4.24; the integrand that specifies R contains the diameter raised to 3.67. Hence an almost linear relationship between K_{DP} and R follows (Sachidananda and Zrnic', 1985).

Balakrishnan et al. (1988a) have examined error statistics due solely to the DSD variations. They used actual DSD's collected with a disdrometer from several Oklahoma storms. A summary of their results is contained in Table 1. Radar rain rates were simulated from disdrometer derived DSD's as indicated in the table. AAD refers to the average absolute deviation between simulated and actual values, and RMS(R) are root-mean-squared values; both of these are

normalized by the rain rate. Besides Marshall-Palmer the best fit Z_H,R relation is also used to indicate the most that can be achieved with this single parameter method. In an operational environment the best fit could be provided by rain gages or disdrometers. The two polarimetric methods were simulated, Eqs. (1.2) and (1.3), with the assumption that the maximum diameter could be either 7 mm or 5 mm. The smaller diameter was more realistic for the particular data as indicated by 1) the disdrometer and 2) the reduced errors in estimates (Table 1). A choice of a smaller maximum diameter requires slight change in empirical relationships that may not be very practical.

Table 1

Comparison of Algorithms for Rainfall Estimation

Rainfall Estimator	Maximum Diameter	Average Absolute Deviation, AAD	Normalized Root-Mean-Squared RMS(R)
$R(Z_H)$; $(Z_H = 200\ R^{1.6})$	Not applicable	0.36	0.4
Best fit Z_H, R		0.19	0.34
$R(Z_H,Z_{DR})$	7 mm	0.18	0.22
$R(K_{DP})$		0.13	0.15
$R(Z_H,Z_{DR})$	5 mm	0.1	0.15
$R(K_{DP})$		0.08	0.1

Examinamation of Table 1 indicates that the Z_H,Z_{DR} method offers some improvement over the best fit Z_H method. K_{DP} produces more significant improvement and as theory predicts is less sensitive to the DSD parameters (in this case assumed maximum drop diameter). Other investigators (Goddard and Cherry,

1984; Ulbrich and Atlas, 1984) have obtained very similar results for the two reflectivity based measurements.

Because Z_{DR} is used to determine the exponent of a drop size distribution with the assumption of an equilibrium axis ratio model, any change in Z_{DR} due to axis ratio change reflects as a drop size distribution exponent change which will create large errors in rainfall rate. If there exists significant natural variability in the axis ratios (15%), the error in $R(Z_H, Z_{DR})$ due to the assumption of equilibrium axis ratios (or any other fixed relation), may exceed the error in the simple Z_H,R relation. The problem is further compounded whenever mixed phase hydrometeors are present.

Next we shall examine the errors due to the statistical uncertainty of the measurements. It is straightforward to obtain expressions for these errors by expending to first-order Eqs. (1.1), (1.2) and (1.3). In deriving the expression for the error in the $R(Z_H,Z_{DR})$ we assume that the rain rate is related to Z_H by the Marshall-Palmer Formula (1.1); this then forces a relationship between Z_{DR} and Z_H. Radar estimates of these two quantities are statistically uncorreleted (Chandrasekar and Bringi, 1986) which is one of the reasons that the rain rate error increases. When measurement errors are summed in a mean square sense with errors due to DSD variations the following normalized expressions are obtained:

$$\frac{SD\,[R\,(Z_H)\,]}{R} = [0.02\ VAR\,(Z_H\,) + RMS^2(R)\,]^{0.5} \qquad (1.4)$$

$$\frac{SD\,[R\,(Z_H,Z_{DR}\,)\,]}{R} = [\frac{8\ VAR\,(Z_{DR}\,)}{R^{0.8}} + 0.053\ VAR\,(Z_H\,) + RMS^2(R)\,]^{0.5} \qquad (1.5)$$

$$\frac{SD[R(K_{DP})]}{R} = \left[\frac{790\ VAR(K_{DP})}{R^{2.3}} + RMS^2(R)\right]^{0.5}. \qquad (1.6)$$

In these expressions the variances are for a resolution cell (in the example to follow it is over 4 range locations). Units for Z_H, Z_{DR}, K_{DP} and R are dBZ, dB, deg km^{-1} and mm h^{-1}; RMS(R) refers to the appropriate uncertainty caused by the variability of the DSD as quantified in Table 1. For illustration we will take the RMS values of .4 for the Marshall-Palmer relationship, .22 for the Z_H, Z_{DR} method and .15 for the K_{DP} method. Assuming that averaging is done over four samples in range, and that the Doppler spectrum width is 2 m s^{-1} (in Section 3 we will use the NTR benchmark spectrum width of 4 m s^{-1}), we take from Section 2.2.7 the standard deviations of Z_H, Z_{DR}, and K_{DP} to be .725 dBZ, .1 dB and .66 deg km^{-1}. This then allows us to plot Eqs. (1.4), (1.5) and (1.6) in Fig. 1.1. It is significant that $R(K_{DP})$ outperforms the other two methods at larger rain rates (> 43 mm h^{-1}) because then, the total amounts are larger and thus more critical for accurate flash flood forecasts.

Two more advantages of the K_{DP} measurements are: 1) that incomplete beamfilling does not degrade the rain rate as happens to reflectivity based methods and 2) that they are independent of the power calibrations.

Comparisons performed so far are valid for pure rain. Presence of ice and rain mixtures complicates rainfall estimation and may cause grave errors. Also it is important to identify the type of hydrometeors within the resolution volume in order to use a proper relationship such as for example Z,R for wet or dry snow, etc. Research in these areas of polarimetric measurements is still very active (Bringi et al., 1986; Balakrishnan et al., 1988b) and some of it is addressed in the next section.

1.2 Discrimination between hail and rain

Remote discrimination between hail and rain using dual polarization measurements is based on the difference in shape, orientation and size distribution of raindrops and hail stones. Z_{DR} values in regions of rainfall range from 0.5 to 4 dB; the larger Z_{DR} generally correspond to larger Z_H. However, radar measurements indicate that when hail is likely, Z_H is high and Z_{DR} is low (Bringi et al.,1984). This has lead Aydin et al. (1986) to define a function of Z_H and Z_{DR} which they call "hail signal," H_{DR}. H_{DR} is a difference between the reflectivity Z_H (for a given Z_{DR}) and the reflectivity for the same Z_{DR} at a boundary between rain and hail defined by:

$$Z_H = \begin{cases} 20\, Z_{DR} + 20 & \text{for} \quad 0 < Z_{DR} \leq 2 \text{ dB} \\ 60 & \text{for} \quad 2 < Z_{DR} \end{cases} \tag{1.7}$$

This boundary was determined from ground based disdrometer measurements. In contrast, Leitao and Watson (1984) used actual radar observations to define a more suitable boundary as:

$$Z_H = \begin{cases} -4Z_{DR}^2 + 19Z_{DR} + 37.5 & \text{for} \quad 0 < Z_{DR} < 2.5 \text{ dB} \\ 60 & \text{for} \quad 2.5 < Z_{DR} \end{cases} \tag{1.8}$$

A scattergram of Z_H, Z_{DR} values in Fig. 1.2 shows the departure from the boundaries for an Oklahoma hailstorm (Steinhorn and Zrnic', 1988).

Lipschutz et al. (1986) have categorized hail size and rain intensity with the help of boundary (1.8) and have produced a precipitation type intensity product based on partitions of the Z_H, Z_{DR} plane as in Fig. 1.3(a). They have operationally tested the probability of hail detection (POD) on the ground and have obtained a POD of 0.56, which is slightly lower than the 0.68 value they obtained with the NEXRAD hail algorithm.

Balakrishnan et al. (1988b) not only proposed a discrimination using a boundary in the Z_H, K_{DP} plane but also proposed quantification of the rain and hail mixture. A discriminant for rain and hail together with a partition of the K_{DP}, Z_H plane according to rain and hail type (analogous to the one in the Z_{DR}, Z_H plane) is shown in Fig. 1.3(b). The empirical curve delineating rain from hail region is given by:

$$K_{DP} = 10^{(Z_H - 45)/12.5} \quad (\text{deg km}^{-1}). \tag{1.9}$$

In the next section we offer heuristic arguments for use of K_{DP} for estimating liquid water in a mixture of rain and hail.

1.3 Quantification of rain and hail rates

The three polarization parameters, Z_H, Z_{DR} and K_{DP} can be used to estimate the relative, and with some assumption, absolute amounts of rain and hail in a mixture. We examine this premise with a simple, but physically appealing theory and indicate extensions that can produce better results.

Consider a homogeneous mixture of isotropic and anisotropic scatterers along a propagation path (Fig. 1.4). Let the ensemble average of the two-way differential propagation phase constant for vertical polarization be $\langle k_v \rangle$ and for horizontal $\langle k_h \rangle$. Without loss of substance attenuation can be neglected and these phase constants can be written as (Oguchi, 1983):

$$\langle k_V \rangle = k_o + \langle k_{Vr} + k_{Vh} \rangle \tag{1.10a}$$

$$\langle k_H \rangle = k_o + \langle k_{Hr} + k_{Hh} \rangle \tag{1.10b}$$

where k_o is the free-space propagation constant, k_{Vr} and k_{Vh} are contributions by rain and hail to the constant for vertically polarized waves and k_{Hr} and k_{Hh} are similar contributions for horizontally polarized waves. Now for isotropic hail $\langle k_{Vh} \rangle = \langle k_{Hh} \rangle$ so that after subtracting (1.10a) from (1.10b) the two-way differential propagation constant becomes:

$$K_{DP} = 2(\langle k_H \rangle - \langle k_V \rangle) = 2(\langle k_{Hr} \rangle - \langle k_{Vr} \rangle). \qquad (1.11)$$

This remarkable yet simple result states that the differential propagation constant is affected by anisotropic scatterers only, in this instance rain. The physical explanation behind this fact is trivial, namely isotropic scatterers produce equal phase shifts for either polarization and the difference is due only to the nonisotropic constituents of the medium. Nonspherical hailstones behave as isotropic scatterers if they tumble. thus propagation phase shift is not dependent on polarization. Even for statistically anisotropic hail mixed with rain the K_{DP} will be mainly affected by rain drops if the water coating on hailstones is sufficiently thin. That is caused by a considerably lower refractive index of ice and lower number density of hailstones.

To obtain the portion of reflectivity factor due to hail one needs to subtract from the measured Z_H the part produced by rain, Z_{Hr}. A direct estimate of Z_{Hr} is not available, but an indirect one may be obtained from the rain rate via a Z_{Hr},R relationship.

We use (1.3) and the Marshall-Palmer Z_{Hr}, R formula to obtain a Z_{Hr}, K_{DP} relationship

$$Z_{Hr} = 24800\ (K_{DP})^{1.386} \qquad (mm^6\ m^{-3}). \qquad (1.12)$$

Now reflectivity factor of hail is estimated as

$$Z_{Hh} = Z_H - Z_{Hr} \qquad (mm^6\ m^{-3}). \tag{1.13}$$

From Z_{Hh} and an appropriate hail distribution such as given by Cheng and English (1983) the rate of hail fall is estimated.

Theoretical relationships between K_{DP} and Z_H for various ratios of hail rate (in mm h^{-1} of equivalent liquid water) are shown in Fig. 1.5(a). Spherical shape for hailstones is assumed and dielectric constants of pure water and dry ice are used in the extended Waterman T matrix method to obtain these curves. Assumed are a Marshall-Palmer DSD (N_0 = 8000 mm^{-1} m^{-3}) and a Cheng-English hailstone distribution ($N(D) = N_0 \exp(-\lambda D)$; $N_0 = 115\ \lambda^{3.63}$ in mm^{-1} m^{-3} for λ in mm^{-1}). Examination of data stratified in the vertical reveals the general trend towards larger proportion of ice with height as expected (Fig. 1.5(b)). No independent confirmation of the relative concentrations was possible.

To check the consistency of this method one may also compute the rain rate from the pair Z_{Hr}, Z_{DRr} where Z_{DRr} is the differential reflectivity due to pure rain. It is contained in the expression for the Z_{DR} of the mixture

$$Z_{DR} = \frac{Z_{Hh}+Z_{Hr}}{Z_{Vh}+Z_{Vr}}. \tag{1.14}$$

Now for isotropic scatterers $Z_{Hh} = Z_{Vh}$; Z_{Hr} is given by (1.12) so that Z_{Vr} can be computed from (1.14) and hence Z_{DRr}. The rain rate is then estimated from (1.2).

Two limitations are associated with the estimate of hail reflectivity. First, the Marshall-Palmer relationship may not be appropriate for a

particular rain/hail mixture, in which case an unknown bias will be present. Second, errors in Z_H will cause errors in Z_{Hh}. These can be controlled because they depend on the number of samples, Doppler spectrum width, and other known or assumed parameters.

Data from a storm that occurred over Norman, Oklahoma on May 14, 1986 is presented to discuss some of our stipulations. Two sample plots of Z_H, K_{DP} and Z_{DR} are shown in Figs. 1.6(a) and 1.6(b). These were collected with a radar that was scanning in an RHI mode from 40 km away. An average over 2.4 km in range was performed.

In Fig. 1.6(a) the vertical profile of Z_H shows that 45 dBZ level is at an altitude of 9 km, indicating a high probability of occurrence of hail on the ground (Waldvogel et al., 1979). Z_H increases around 3.2 km from which the onset of melting could be inferred. The differential reflectivity Z_{DR}, is zero from about 2.8 km up to the cloud top. This could correspond to tumbling or spherical hail also in conformity with K_{DP} profile that is zero above 4 km. With the onset of melting in tumbling hail, liquid water builds up around the equator of hailstones and small water drops are shed that may coalesce to produce larger drops. Also, smaller hail and snow aggregates melt totally or partially and still retain oriented oblate shape before larger hailstones melt. As soon as there is a small amount of oblate wet (or melted) hydrometeors, the K_{DP} begins to increase. However, Z_{DR} changes only after a larger number of such hydrometeors are formed. This is due to the fact that Z_{DR} depends on the axis ratio and reflectivity combinations of both rain and hail being weighted more towards the axis ratio of higher reflectivity hailstones, whereas K_{DP} is not affected by the presence of hail.

At the onset of melting Z_{DR} is dominated by contributions from hail and is insensitive to the few raindrops. As melting proceeds more drops are

generated and Z_{DR} begins to grow. Thus there is a 1 km lag between the altitudes at which Z_{DR} and K_{DP} start to increase. This lag would depend on the hail reflectivity and the rate at which water drops are generated. It should be remarked here that although the small negative excursions of K_{DP} above 8 kms altitude are within the experimental accuracies of K_{DP} measurement their consistency suggests presence of vertically oriented hydrometeors--possibly graupel.

Below the melting layer K_{DP} follows nearly the variations of Z_H which decreases marginally at 1.8 km due to change in fall velocity which acts to decrease the drop concentration (Battan et al., 1973). The marginal decrease in Z_H, and the steady increase in Z_{DR} suggest progression of melting up to the ground level, a fact confirmed by observation of hail and rain mixture at the ground.

The correlation $|\rho_{HV}(o)|$ begins a systematic decrease at about the altitude where K_{DP} starts increasing. Theory predicts the decrease until the power contributed by rain backscatter is roughly equal to the power contributed by hail backscatter (see Sec. 3.4 and Fig. 1.9). A hydrometeor ensemble of either pure small hail or pure rain has larger $|\rho_{HV}(o)|$ than the mixture. This is because the main cause for decorrelation is from the distribution of scatterers that introduces a distribution of axial ratios. The presence of two types of hydrometeors broadens the distribution of sizes and thus increases the decorrelation.

Figure 1.6(b) shows the vertical profiles of Z_H, Z_{DR} and K_{DP} and $|\rho_{HV}(o)|$ at the tail end of the storm. The 45 dBZ layer is at a lower altitude of around 4 km. There is no significant lag in altitudes at which Z_{DR} and K_{DP} start to increase, indicating a low concentration of hail aloft. A more pronounced peak in Z_H profile showing the effects of changes in fall velocity

characterizes a very low, if any, hailfall rate at the ground. At the earlier time (Fig. 1.6(a)) small hail (1 cm) mixed with rain was observed on the ground. Later (Fig. 1.6(b)) there was no hail on the ground.

Shown in Fig. 1.7 are variations of rain and hail rates with time. Data are averaged over 1 km in range and altitudes between .1 and 1 km. The sharp drop at 10 minutes (relative to 16:55:00) occurred when hail essentially ceased at the ground. Rain rate computed from Marshall-Palmer relationship (1.1) using total reflectivity Z_H exceeds the rate obtained from $R(K_{DP})$ (1.3). A nearby gage on the ground gave close agreement with $R(Z_H)$. This is because the weighing bucket gage measured both liquid and water from melted ice. Rain rate $R(Z_H, Z_{DR})$ without correction of Z_{DR} for hail gave grossly exaggerated values, four to five times larger. A simple correction of Z_H and Z_{DR} (1.12, 1.13) produces a credible rain rate of liquid water (Fig. 1.7). A more complicated procedure (not shown) was also tried whereby the differential propagation phase constant was adjusted to account for presence of small oblate hail. Then the derived rain rate agreed extremely well with $R(K_{DP})$.

1.4 Discrimination of hail sizes

Besides separating rain from hail in the mixture of the two, polarization measurement allows quantification of hail size. One method uses partitions of the Z_H, Z_{DR} plane or Z_H, K_{DP} plane (Figs. 1.3(a) and 1.3(b)) to establish presence of hail and the Z_H values to gauge size. But because both concentration and size determine the reflectivity factor the estimated size is not reliable. Here we explore an alternate approach that is based on the following three physical premises.

One is the observation (List, 1983) that larger hailstones (4-10 cm in diameter) are roughly irregular, with small or large protuberances. That is

to say, hailstones do not obey fractal laws so the protuberance to diameter ratio is not constant but may increase with size. Although this is not always the case, when true it will result in a noticeable decrease of $|\rho_{HV}(o)|$. It can be shown that the correlation coefficient for monodispersed Rayleigh scatterers with random Gaussian protuberances is given by the following formula:

$$|\rho_{HV}|(o)| = (1 + 3\sigma_D^2/D^2)^2 / (1 + 15\sigma_D^2/D^2 + 45\sigma_D^4/D^4 + 15\sigma_D^6/D^6), \qquad (1.15)$$

where σ_D is the rms value of the protuberance and D is the diameter of a sphere with volume equal to the hailstone. Plot of this equation (Fig. 1.8) indicates that a σ_D/D of 0.1 may reduce the correlation to 0.92. Calculations need to be performed with formulas valid for Mie scattering and realistic distributions to quantify more precisely the effects of irregularities on large hailstones.

The second premise is rooted in the fact that below the melting layer there will be rain mixed with hail. It is a fact that a distribution of sizes, shapes, canting angles and phase shift upon scattering from hydrometeors consisting of a mixture of rain and hail broadens with increasing hail size thus decreasing correlation. In Fig. 1.9 we have plotted the correlation coefficient for a mixture of rain and hail. It is assumed that the rain rate is 40 mm h^{-1} and that hail rate is variable. Rain is modeled with a Marshall-Palmer drop size distribution, and hail with a Cheng-English distribution of sizes. The model for hail consists of oblate spheroids whose minor axis are horizontally aligned. As seen in Fig. 1.9, the correlation does drop with increasing hail rate (and thus size). Also the decrease is not monotonic, but exhibits an oscillation that could introduce an ambiguity in inferred hail sizes.

The third premise is that larger sizes of spongy hailstones produce rapid oscillations in the Z_{DR} with change in diameter due to Mie scattering (Longtin et al., 1987). This tends to decrease the correlation.

All of these three premises may be simultaneously valid but our very limited experience is that mixed phase is definitely one of the factors. Aerodynamic considerations (Knight and Knight, 1970) suggest that hailstones larger the about 2 cm are elongated in the direction of fall. Still larger sizes of spongy hail produce rapid oscillations in the Z_{DR}. Both of these effects act in the same direction tending to reduce the correlation especially when phases are mixed. Note that this tendency is practically insensitive to the distribution of liquid water, i.e., it is the maximum hailstone size that broadens the composite distribution. We note here that the differential reflectivity is an ambiguous indicator of hail size and orientation because in the Mie regime of scattering it changes sign in a complicated manner.

Comparisons between vertical profiles of polarimetric parameters Z_H, Z_{DR}, K_{DP} and $|\rho_{HV}(o)|$ measured in a storm of June 2, 1985 (Fig. 1.6) and May 14, 1986 (Fig. 1.6(a)) show some similarities and also significant differences. Walnut hail size was observed on the ground on June 2 but smaller than 1 cm hail fell at the location of data collection on May 14. Reflectivity factor profiles are very similar and on the basis of these one would expect little difference in precipitation type and size. But differences in the other measurables point out that hail was larger on June 2. Negative Z_{DR} extends to 10 km suggesting larger vertically aligned hailstones on June 2; K_{DP} increases from the top of the melting layer to the ground indicating the dominant effect of melting as opposed to break up and coalescence which might explain the profile decrease of K_{DP} below 1.5 km in Fig. 1.6(a).

Below the melting layer Z_{DR} grows monotonically indicating ongoing melting process and dominance of oblate hydrometeors on May 14. The negative Z_{DR}, all the way to the ground, on June 2, suggests that liquid drops and other small (< 3 cm) horizontally elongated hydrometeors contribute little to it. Most striking is the systematic decrease of $|\rho_{HV}(o)|$. Because the decrease starts at the melting layer on both days, we conclude that the presence of mixed phase hydrometeors is mainly responsible. As expected with larger hail sizes (Fig. 1.10) the decrease is significantly bigger.

Above the melting layer the correlation coefficient for the June 2 storm is consistently but slightly smaller (by about 0.01) than the correlation for the May 14 storm. This could be explained by either protuberances or wobbling (or both), and it is certainly consistent with hail size. Nevertheless, it remains to be seen if such small differences above the melting layer are significant, and if so, can they be reliably estimated.

1.5 Conclusions

It is submitted that the differential measurements will provide new information about the meteorology which will significantly enhance the NEXRAD performance by:

- reduced dispersion (standard deviation) of rainfall rate measurements,
- improved rainfall rate measurement of the higher rates ($R > 40$ mm hr^{-1}),
- distinguishing between liquid water and hail, and
- possible ability to gauge hail size.

In Section 2 we present a processing scheme which allows the differential measurements to be made without compromising the radar's prime mission.

2. Signal Processing

Doppler weather radar generally provides the first three spectral moments of the echo signal from which the three commonly used observables, namely the reflectivity (Z), the velocity (v) and the spectrum width (σ_v) are derived. Polarization switching adds another dimension to signal processing that must be dealt with. Because rain drops are oblate and nearly oriented with the axis of symmetry along the vertical, the radar cross section is different for the two polarizations and so is the propagation constant through rain. Amplitude and phase modulation of the time series samples at the polarization switching frequency thus result. The amplitude modulation can be related to Z_{DR} and the phase modulation to ϕ_{DP}.

To estimate Z_{DR} and ϕ_{DP}, together with Doppler parameters, requires accounting for this modulation, either in the autocovariance or spectral domain. This fact was recognized by Metcalf and Armstrong (1983) who suggested transmission sequences consisting of few consecutive pulses with equal polarization in which the modulation does not affect the autocovariance. Such sequences are suboptimal with respect to errors in polarization variables. It is these errors that dictate needed dwell time, because when they are satisfactory (e.g., less than 0.1 dB for Z_{DR} and less than 1 deg for ϕ_{DP}), errors in Doppler parameters are also acceptable (less than 1 m s^{-1} for velocity and spectrum width), but not vice versa. Hence, any serious attempt to introduce polarization measurements into the operational arena hinges on the ability to generate polarization measurements at rates commensurate with Doppler measurements. The same holds true for research applications in which three-dimensional microphysical and dynamic properties of storms are required. Thus, it is compelling to devise short transmission sequences for which polarization errors are minimized and Doppler estimates are not compromised. This

is precisely what Sachidananda and Zrnic' (1985) achieved with an alternating sequence of linearly polarized (at 45° and -45° from the vertical) waves. But this sequence requires two well-balanced (in amplitude and phase) receivers and appears to be suitable for compensation of propagation effects; neither of these have been demonstrated. For practical and technical reasons, receivers which process vertically, horizontally, or circularly polarized echoes are presently the choice of the radar meteorology community. Minimum variance considerations for Z_{DR} imply that, of all sequences consisting of horizontally and vertically polarized waves, the optimal is the one with alternating polarizations (Fig. 2.1), because the correlation coefficient obtained from such a sequence is largest.

Due to the polarization switching and the consequent modulation, the spectrum of a radar signal with alternating polarization exhibits two peaks separated by half the Nyquist interval (Carter et al., 1986). This necessitates modifications in the normal computation procedure for the estimation of reflectivity, velocity, and spectrum width. Sachidananda and Zrnic' (1988) show theoretically, and in the data, what modifications are needed so that unambiguous differential phase and valid velocity estimates can be retrieved. We briefly review and discuss the implication of their results.

2.1 Doppler parameters

Basically, a sequence of samples, known as the time series, is all that a radar provides for each resolution volume. From these samples all the information about the scatterers in the resolution volume is derived.

In a Doppler radar without polarization diversity the most important meteorological information is obtained from the first three moments of the the power spectrum of the time series data. The reflectivity is calculated from

the mean sample power, or the zeroth moment, mean radial velocity from the first moment of the normalized power spectrum and the spectrum width, which is a measure of the turbulence and/or shear in the resolution volume, is the square root of the second moment of the power spectrum about the mean radial velocity.

Because of the statistical nature of weather echoes, one needs to obtain estimates of spectral moments using several samples. The mean sample power S from a range r_o is estimated using

$$\hat{S} = \frac{1}{M} \sum_i |E_i|^2, \tag{2.1}$$

where M is the number of samples averaged, and E_i are echo sample voltages (either H or V samples).

The mean radial velocity and spectrum width can be estimated using autocovariance processing, that is simpler computationally than the spectral processing. In the autocovariance method the mean velocity obtained by a radar with wavelength λ is given by:

$$\hat{v} = -(\lambda/4\pi T_s) \arg[\hat{R}(T_s)], \tag{2.2}$$

where the autocorrelation estimate $\hat{R}(T_s)$ for lag time T_s is

$$\hat{R}(T_s) = \frac{1}{M} \sum_{i=1}^{M} E_i^* E_{i+1}. \tag{2.3}$$

The spectrum width is also calculated from $\hat{R}(T_s)$ and $\hat{S}$ using

$$\hat{\sigma}_v = \frac{v_a\sqrt{2}}{\pi} \left| \ln\left(\frac{\hat{S}}{|\hat{R}|}\right)\right|^{1/2} \operatorname{sgn}\left[\ln\left(\frac{\hat{S}}{|\hat{R}|}\right)\right], \tag{2.4}$$

where v_a is the Nyquist velocity equal to $\lambda/(4T_s)$. A detailed treatment of estimators of Z, v and σ_v and their standard errors, is given in Doviak and Zrnic' (1984).

2.2 Doppler and polarization parameters

A radar capable of transmitting two linear polarizations provides several additional parameters of interest to the meteorologist. We are concerned here with only three of these, namely the differential reflectivity (Z_{DR}), the differential phase shift (ϕ_{DP}), and the correlation coefficient $\rho_{HV}(o)$. The alternate polarization switching, that enables us to estimate these three additional polarization dependent parameters, also affects the estimation of the three conventional parameters. The fourth parameter, differential propagation constant, K_{DP}, is linearly related to ϕ_{DP}. In the following, the estimation of each of these radar observables using dual polarized radar, is discussed.

2.2.1 Reflectivity and differential reflectivity

The primary intended use of the Z_{DR} is for identification of hail and accurate rainfall estimation. To estimate rainfall rate more accurately using the Z_{DR} method, than that given by an R(Z) relation, errors in Z_{DR} must be less than 0.1 dB, and errors in the reflectivity for the horizontally polarized field (Z_H) must be below 1 dBZ (Sachidananda and Zrnic', 1985). So, the number of samples needed for averaging is dictated by these accuracy requirements.

The most efficient estimate of Z_{DR} uses separate calculations of the powers $\hat{S}_H$ and $\hat{S}_V$ for the two polarizations (Sirmans and Dooley, 1986). If samples from the linear receiver are used, Z_H and Z_{DR} are estimated from

$$\hat{S}_H = \frac{1}{M} \sum_{i=1}^{M} |H_{2i}|^2, \tag{2.5a}$$

$$\hat{S}_V = \frac{1}{M} \sum_{i=1}^{M} |V_{2i+1}|^2, \tag{2.5b}$$

and

$$\hat{Z}_{DR} = 10 \log \left(\frac{\hat{S}_H}{\hat{S}_V}\right) \text{(dB)}. \tag{2.6}$$

Here, M is the number of sample pairs. It may be noted that the number of samples available for $\hat{S}_H$ or $\hat{S}_V$ estimation is half of the total available in a mono-polarized radar, over the same time interval. However, the increase in the standard error due to this reduced number is usually very small because, for a sufficiently large M, the standard error is a function of the total sampling time and the decorrelation time of the signal, which remain unaltered.

Figures 2.2 and 2.3 show the standard errors σ_z and σ_{DR} in $\hat{Z}_H$ and $\hat{Z}_{DR}$ respectively, as a function of the number of samples averaged. These errors are computed from the following equations (Sachidananda and Zrnic', 1985):

$$\sigma_z = 10 \log [1 + SD(\hat{S}_H)/\hat{S}_H] \quad \text{(dB)} \tag{2.7a}$$

and

$$\sigma_{DR} = 10 \log [1 + SD(\hat{S}_H/\hat{S}_V)/(\hat{S}_H/\hat{S}_V)] \quad \text{(dB)}. \tag{2.7b}$$

The spectrum width of the signal is shown as a parameter. It is obvious from a comparison of these two figures that the standard error in Z_{DR} dictates the number of samples required for improved rain rate estimation or discrimination of hail.

2.2.2 Mean radial velocity and differential propagation phase shift

The mean radial velocity and the differential propagation phase shift are obtained from phases of the received echo samples. The weather echo sample spectra can be approximated by a Gaussian shape in most cases. For such spectra the mean radial velocity, v, and the spectrum width, σ_v, are normally estimated using the autocovariance and the mean sample power estimates (Eqs. 2.2, 2.4). Estimators (2.2) and (2.4) do not perform satisfactorily when applied to alternately polarized radar signals. The reason for this becomes clear from an examination of the autocovariance of these signals.

With alternate polarization switching, the autocorrelation estimate using the conventional (pulse pair) processor can be expressed as:

$$\hat{R}(T_s) = \frac{1}{2M} \sum_{i=1}^{M} (H_{2i}^* V_{2i+1} + V_{2i+1}^* H_{2i+2}). \tag{2.8}$$

Summing the two products in (2.8) separately, and representing them by $\hat{R}_a$ and $\hat{R}_b$, we have

$$\hat{R}_a(T_s) = \frac{1}{M} \sum_{i=1}^{M} H_{2i}^* V_{2i+1}, \tag{2.9}$$

$$\hat{R}_b(T_s) = \frac{1}{M} \sum_{i=1}^{M} V_{2i+1}^* H_{2i+2}, \tag{2.10}$$

and

$$\hat{R}(T_s) = \frac{1}{2} [\hat{R}_a + \hat{R}_b]. \tag{2.11}$$

True values of estimates $\hat{R}_a$ and $\hat{R}_b$ are the expected values of products $H_n^* V_{n+1}$ and $V_n^* H_{n+1}$, respectively. It can be shown (Sachidananda and Zrnic', 1988) that the phase of R_a is the sum of phases due to the Doppler shift, $\psi_d = -2T_s(k_o+k_h)v$, and the two-way differential propagation phase shift,

$\phi_{DP} = 2(k_h - k_v)r_o$; whereas, the phase of R_b is the Doppler phase, ψ_d, minus the ϕ_{DP}. k_H and k_V are increments (for horizontal and vertical polarizations) to the free space propagation constant k_o due to the presence of hydrometeors. Thus, we can write the expected (or true) $R(T_s)$ as:

$$R(T_s) = \frac{1}{2}\left[|R_a| e^{j(\psi_d + \phi_{DP})} + |R_b| e^{j(\psi_d - \phi_{DP})}\right]. \tag{2.12}$$

The magnitudes of R_a and R_b are equal (see also Metcalf and Armstrong, 1983), and we simplify (2.12) to:

$$R(T_s) = |R_a| \cos(\phi_{DP}) e^{j\psi_d}. \tag{2.13}$$

This equation holds approximately for the estimates as well. Thus, we can estimate the Doppler phase shift ψ_d using the conventional autocovariance processor only when ϕ_{DP} is less than 90°.

Sachidananda and Zrnic' (1988) have developed a modified estimator to extract the correct velocity along each radial. It not only removes a noisy band in the velocity estimate when ϕ_{DP} is near 90°, but also enables one to resolve the velocity ambiguity caused by ϕ_{DP}. A suggested estimator for ϕ_{DP} is:

$$\hat{\phi}_{DP} = \frac{1}{2} \arg(\hat{R}_a \hat{R}_b^*). \tag{2.14}$$

Figure 2.4 gives the standard error performance of the estimator versus the number of sample pairs averaged to determine $\hat{R}_a$ and $\hat{R}_b$ (Sachidananda and Zrnic', 1986).

Differential phase shift computed from (2.14) is ambiguous when the actual value is outside a 180° interval, but it is easy to resolve this ambiguity knowing that ϕ_{DP} is always positive in the rain medium, and is a monotonically increasing function of range. As a matter of fact, the majority of hydrometeor types would produce either positive or zero differential phase shift. Only vertically oriented particles, such as graupel, produce negative ϕ_{DP}. If the differential phase shift in the radar system is adjusted to zero, ϕ_{DP} will be zero for a path void of hydrometeors and will increase only when the propagation path encounters precipitation. Thus, it is tempting to locate the unambiguous 180° interval from 0° to 180°, and use continuity of ϕ_{DP} in range to correct the ambiguity whenever two consecutive values differ by a large amount (e.g., more than 90°). But at close range ϕ_{DP} is small or zero and statistical uncertainty may produce negative values that must not be changed. Thus, range dependent correction procedure should be used on ϕ_{DP} data.

The velocity should be computed from:

$$\hat{v} = -\frac{v_a}{\pi} \arg[\hat{R}_a \exp(-j\hat{\phi}_{DP})], \tag{2.15}$$

where $\hat{\phi}_{DP}$ is the corrected (unambiguous) value. Multiplication with the exponent in the argument permits vectorial adjustment of the phase of $\hat{R}_a$ so that even for angles larger than 180° a correct (within $\pm v_a$) velocity is obtained.

In Fig. 2.5 we show plots of consecutive complex product vectors $(H_i^* V_{i+1})$ and $(V_{i+1}^* H_{i+2})$, for one time series record with 256 samples. Each point corresponds to the tip of a product vector and the axes are in arbitrary units. The figure indicates clearly that the product vectors form two distinct groups. In fact, all the vectors in the upper half are $(H^* V)$ products and the

ones in the lower half are $(V^{*}H)$ products; the mean of these two groups represent $\hat{R}_a$ and $\hat{R}_b$, respectively. The remarkable similarity in the pattern of distribution of the component vectors of $\hat{R}_a$ and $\hat{R}_b$ is due to the high correlation between H and V samples $(|\rho_{HV}(0)|^2 \approx 0.995)$. The inference from (2.13) that the conventional (pulse pair) mean velocity estimate would be noisy if ϕ_{DP} is near 90°, is obvious in this figure. If $\phi_{DP} = 90°$, the two mean vectors $\hat{R}_a$ and $\hat{R}_b$ exactly oppose each other making the sum nearly zero. The angular spread of the component vectors in each group is a measure of the spectrum width of the signal.

From our analysis we can infer that, if the differential propagation phase shift is around 90°, there will be a region of discontinuity in the velocity estimates along a radial. This is clearly shown in Fig. 2.6, in which we have plotted: 1) the conventional pulse pair velocity estimate (2.2) the velocity derived from a modified estimator (2.15), and 3) the corresponding differential propagation phase shift $\hat{\phi}_{DP}$, along a radial; all parameters have been calculated from time series records. Note that the conventional pulse pair estimator and the modified estimator give the same velocity value as long as $\hat{\phi}_{DP}$ is less than 90°; when $\hat{\phi}_{DP} \approx 90°$, conventional pulse pair estimates become noisy, and for $\hat{\phi}_{DP} > 90°$, the velocity shifts by v_a, the Nyquist velocity.

2.2.3 Differential propagation constant

Differential propagation constant is defined as a difference between propagation constants for horizontally and vertically polarized electromagnetic waves. In a homogeneous medium, it can be directly obtained from differential phase shifts at two range locations,

$$K_{DP} = \frac{\phi_{DP}(r_2) - \phi_{DP}(r_1)}{r_2 - r_1} \tag{2.16}$$

In practice K_{DP} should be estimated from measurements at several contiguous range locations r_i. Although this does reduce the resolution it serves to decrease the errors of estimates. Because in a homogeneous medium $\phi_{DP}(r_i)$ is linearly related to K_{DP}, a least-squares-fit is recommended for estimating K_{DP}. Thus at a center range r_o given by

$$r_o = \sum_i r_i / L, \tag{2.17}$$

where L is the number of range gates for averaging, the least squares solution for $\hat{K}_{DP}(r_o)$ is:

$$\hat{K}_{DP}(r_o) = \frac{\sum[\phi_{DP}(r_i) - \overline{\phi_{DP}}(r_i)]\,(r_i - r_o)}{\sum_i (r_i - r_o)^2} \tag{2.18}$$

Note that the overbar in (2.18) denotes the average value over the L range locations. Now the variance of $\hat{K}_{DP}$ is linearly related to the variance σ_ϕ^2 of ϕ_{DP} by:

$$\mathrm{VAR}(\hat{K}_{DP}) = \frac{\sigma_\phi^2}{\sum_i (r_i - r_o)^2} \tag{2.19}$$

2.2.4 Spectrum width

Weather signals normally have Gaussian power spectra for which the correlation coefficient for m pulse lag, $\rho(mT_s)$ is (Doviak and Zrnic', 1984):

$$\rho(mT_s) = \exp(-8\pi^2 \sigma_v^2 T_s^2 m^2/\lambda^2) \exp(-j2\pi f_d T_s m) + \delta_m \cdot \mathrm{SNR}^{-1}, \tag{2.20}$$

where σ_v is the spectrum width in (ms^{-1}), f_d is the mean Doppler frequency, and δ_m the Kronecker delta.

In a radar with alternating polarization, samples of equal polarization are available only at a PRT of $2T_s$, thus, $\rho(mT_s)$ is unaffected by switching for even values of m. The spectrum width σ_v can be estimated from $\hat{R}(2T_s)$, but additional computation (over the one for $\hat{R}_a$ and $\hat{R}_b$) is required to estimate $R(2T_s)$. Further, at large spectrum widths the estimate of $R(2T_s)$ is not as good as the estimate of $R(T_s)$, which is readily available in the modified procedure for velocity and ϕ_{DP} processing.

We can express the autocorrelation R_a as:

$$R_a(T_s) = \langle H_i^* V_{i+1} \rangle = (S_H S_V)^{1/2} r_{HV}(T_s), \tag{2.21}$$

where $S_{H,V}$ are the mean powers of H and V samples respectively, and r_{HV} is their correlation coefficient. The samples H_i and V_{i+1} decorrelate mainly due to (a) the Doppler spread, and (b) the drop shape and canting angle distribution (Sachidananda and Zrnic', 1985). Because these two processes can be assumed to be statistically independent, we write:

$$R_a(T_s) = (S_H S_V)^{1/2} \rho(T_s)\, \rho_{HV}(T_s), \tag{2.22}$$

where $\rho(T_s)$ is the correlation coefficient due to the Doppler spread, and $\rho_{HV}(T_s)$ is the correlation coefficient arising from drop shape (via size) and canting angle distribution. We can approximate $\rho_{HV}(T_s) \approx \rho_{HV}(0)$ because the changes in the distributions of drop shape and canting angle are small over the short (~ 1 ms) sampling time. In most cases $|\rho_{HV}(0)|$ is nearly unity (> 0.997) hence, the spectrum width can be estimated from the formula:

$$\hat{\sigma}_v = \frac{v_a\sqrt{2}}{\pi}\left| \ln\left[\frac{\hat{S}_H\hat{S}_V}{|\hat{R}_a\hat{R}_b|}\right]^{1/2}\right|^{1/2} \operatorname{sgn}\left[\ln\left[\frac{\hat{S}_H\hat{S}_V}{|\hat{R}_a\hat{R}_b|}\right]^{1/2}\right]. \qquad (2.23)$$

Note that (2.23) is derived from the conventional spectrum width estimator by replacing $\hat{R}$ by $|\hat{R}_a\hat{R}_b|^{1/2}$ and $\hat{S}$ by $(\hat{S}_H\hat{S}_V)^{1/2}$. There is no noticeable difference in results if the geometric means are replaced with arithmatic means of the magnitudes. For a sufficiently large M, $|\hat{R}_a|$ and $|\hat{R}_b|$ are identical thus, the performance of this estimator would be nearly the same as the conventional one.

2.2.5 Correlation coefficient

Correlation coefficient between H and V echoes, $\rho_{HV}(o)$ depends on the shape, oscillation, wobbling and canting angle distribution of hydrometeors. When transmission consists of alternating H,V samples two assumptions are needed to estimate $\rho_{HV}(o)$. First, some a priori model for the power spectral shape is needed such as Gaussian (2.20). Second, the correlation at a lag $(2m+1)T_s$ is assumed to contain independent contributions from the Doppler spectrum broadening and $\rho_{HV}(o)$ so that it can be expressed as a product $\rho(2m+1)\cdot\rho_{HV}(o)$. The correlation due to the Doppler spread at lag $2T_s$ is:

$$\hat{\rho}(2T_s) = \frac{\sum(H_{2i}H^*_{2i+2}+V_{2i+1}V^*_{2i+3})}{(2M-1)\ (\hat{S}_H+\hat{S}_V)}, \qquad (2.24)$$

and the assumption of Gaussian spectral shape allows equating $|\hat{\rho}(T_s)|$ to $|\hat{\rho}(2T_s)|^{0.25}$. An estimate of $|\rho_{HV}(T_s)|$ is obtained from (2.5a), (2.5b), (2.9) and (2.10)

$$|\hat{\rho}_{HV}(T_s)| = \frac{|\hat{R}_a|+|\hat{R}_b|}{2(\hat{S}_H\hat{S}_V)^{1/2}}, \qquad (2.25)$$

so that the correlation coefficient magnitude $|\hat{\rho}_{HV}(o)|$ is directly computed:

$$|\hat{\rho}_{HV}(o)| = |\hat{\rho}_{HV}(T_s)/\hat{\rho}(T_s)|. \tag{2.26}$$

2.2.6 Radar phase stability requirements

The accuracy of the estimates are dependent on the radar stability as well as signal statistics. The more stringent system requirement for the differential measurements is phase stability.

For example, consider an rms phase fluctuation σ_Δ (in rad.). It can be shown that a signal-to-noise ratio for a pure complex sinusoid subjected to such fluctuations is

$$S/N = \exp(-\sigma_\Delta^2)\,(1 - \exp(-\sigma_\Delta^2))^{-1}. \tag{2.27}$$

Equation 2.27 is plotted in Fig. 2.7 where it is evident that even small phase fluctuations (less than 1°) produce considerable degradation of SNR. In order to measure the differential phase at a point with inherent errors (due to statistical nature of weather echoes) of the order of 1° the phase jitter after coherent integration should be below 0.2°. If 61 pulses are coherently integrated, this translates to a phase jitter of 1.6° and an equivalent SNR of over 30 dB. Because NEXRAD ground clutter specifications stipulate a spectral peak to noise level of over 50 dB (per pulse SNR over 40 dB) the system is inherently capable of achieving the differential measurement.

3. Dual Polarization Engineering Modifications

The dual polarization measurement requires a radar engineered for transmission and reception of linear orthogonal fields. In the NEXRAD radar system

engineering changes are required in the antenna feed, transmitter and receiver switching, signal processing and waveform, and associated timing control logic.

3.1 Antenna and transmitter/receiver

Antenna and transmitter/receiver modifications (Fig. 3.1) consist of the addition of a horizontal/vertical switch and orthomode coupler/antenna feed. The switch is a high speed latching ferite circulator. State of the art switching time for these devices is less than 6 μs, reverse port isolation is greater than 25 dB, and insertion loss is less than 0.75 dB. The orthomode coupler generates either a horizontally or vertically polarized wave depending on which port is exited. State of the art isolation between ports of the coupler is greater than 40 dB. The antenna feed illuminates the reflector with either polarization. The required orthogonal field cross-coupling of less than -24 dB is well within the state of the art and would probably be delivered by the Unisys feed and reflector. The latching circulator insertion loss can be absorbed by the NEXRAD excess detection margin and does not result in a decrease of specified detection capability. No changes are needed in the receiver.

The microwave components required for dual polarization are existing technology (Carter, et al., 1986). Furthermore, all modifications can be accommodated by the NEXRAD without major physical or electrical changes.

3.2 Signal processing

The dual polarization measurement impacts NEXRAD signal processing in the areas of spectral moment estimation, the differential polarization measurements, and also in the processing for clutter suppression.

3.2.1 Spectral moment and differential parameters

The modifications required in the signal processing are an expansion of the processing capability for the differential measurements and a modification of the existing processing scheme for spectral moment estimation.

An alternating polarization signal processing schematic based on the discussion in Section 2 is shown in Fig. 3.2. The Z_{DR} is derived using a square law estimator which has much lower standard error than a logarithmic estimator (Sirmans and Dooley, 1986). The reflectivity is also derived from I and Q samples by a square law estimator. Note the additional accumulator in the reflectivity processor and in the pulse pair processor, to store the values for the two polarizations separately. The calculation procedure for the mean velocity and the spectrum width should be that given by Eqs. (2.15) and (2.23).

Examination of the equation for the differential phase estimator reveals the complexity, i.e., the number of arithmetic operations and storage requirements, to be between that of mean velocity and spectrum width estimation. Signal processing capability expansion is estimated to be 50% to 100% of existing.

3.2.2 Clutter filtering

In Section 2 it is shown that the differential measurements can be made without compromising the spectral moment measurements. However, this is not the case for clutter filtering. A single recursive or finite impulse response filter will not deliver a large suppression on an alternating polarization sequence. Clutter filtering will have to be done on separate H and V pulses. Filtering the polarization separately is equivalent to filtering over half the Nyquist interval (i.e., every other pulse) and will result in a filter notch and associated weather echo bias at the Nyquist midpoint. With this technique

of clutter filtering the spectral moment estimates are degraded when the mean velocity is at the Nyquist midpoint in the same way as when the mean velocity is at zero. (See NTR Tables 3-7 and 3-8). However, there will be no degradation in the magnitude of clutter suppression. System clutter processing expansion requirements are addition of a second clutter filter.

3.3 NEXRAD dual polarization performance

Implementation of the dual linear polarization measurement as proposed in Section 2 will not compromise the spectral moment measurements, i.e., the prime mission of the system. Thus the dual polarization measurements are considered adjuncts to the system and the "goodness" of these estimates will be determined by what can be achieved with system parameters (i.e., PRT, antenna rotation rate, etc.) chosen for spectral moment measurements.

The detailed performance of the overall system under a variety of meteorological conditions can be derived from the analysis given in Section 2.2.6. Two general aspects of the differential estimation performance are noteworthy.

The prime operational parameter determining estimate standard deviation is the radial dwell time. So long as the fundamental constraint of spectrum coherency is satisfied (and it must be for spectral moment estimation) the radar PRF or Nyquist velocity is a secondary influence on estimate accuracy.

There is only a weak dependency of differential estimate accuracy on spectrum width. For example, at the dwell time for 1° samples with rotation rate of 3 rpm and input spectrum width ranging from 2 m s^{-1} to 6 m s^{-1} the differential reflectivity estimate varies about ± 10%, and the differential phase estimate varies about ± 20%.

Thus, if the system is configured to deliver "satisfactory" differential estimator performance under nominal operating conditions it will deliver "satisfactory" performance over the entire range of operating conditions.

"Satisfactory" performance must of course be quantified. System improvement in the case of the differential measurements is in the two general areas of reduced standard deviation of rainfall rate measurements as well as new measurement capability. New measurements provide the capability to distinguish between liquid water and hail and the capability to gauge hail size.

The accuracy required of the estimate is discussed in Section 1.1 and in the literature (Sirmans et al., 1986; Sachidananda and Zrnic', 1987; Balakrishnan and Zrnic', 1988). From these and other considerations we establish the following performance criteria.

For a significant improvement over the conventional method, the accuracy of the differential measurement must be such as to reduce the standard deviation of rainfall estimate by at least one third. This in turn requires the following constraints on the errors: reflectivity estimate standard deviation, $SD[Z_H] < 0.7$ dB, differential reflectivity estimate standard deviation, $SD[Z_{DR}] < 0.1$ dB, and propagation phase shift standard deviation, $SD[K_{DP}] < 0.7$ deg km^{-1}. Estimate accuracy requirements for scatter phase state distinction (i.e., distinguishing between liquid water and hail) are more than satisfied by the rainfall estimate accuracy requirements. From Figs. 1.5 and 1.6 it is seen that a reflectivity estimate standard deviation of 1 dB in conjunction with a phase gradient estimate of 1 deg km^{-1} delineates the rain-hail boundary quite well. In practice the standard deviation could be considerably larger and still provide reliable distinction between the two different types of scatterers.

Discrimination of hail size (Section 1.4) utilizes the correlation coefficient between horizontally and vertically polarized echoes, $|\rho_{HV}(o)|$ in addiion to the Z_H, Z_{DR}, and K_{DP} measurements. Hail size gauging capability remains to be demonstrated. However, preliminary measurements (Figs. 1.6, 1.9, and 1.10) imply a coefficient accuracy of about ± 0.01 (in conjunction with the above accuracies of Z_H, Z_{DR}, and K_{DP}) will be adequate. This requires dwell times compatible with that of Z_H, Z_{DR}, and K_{DP}.

Typical differential measurement performance is shown in Figs. 3.3, 3.4, and 3.5. For the presented conditions and measurements on a 1° by 1 km polar grid at antenna speeds of 1 rpm to 4 rpm the estimated accuracies are: $0.56\ dB < SD[Z_H] < 0.8\ dB$, $0.03\ dB < SD[Z_{DR}] < 0.5$, and $0.45\ deg\ km^{-1} < SD[K_{DP}] < 0.65\ deg\ km^{-1}$.

Estimate accuracy should be sufficient to provide a significant improvement over the conventional methods for all proposed operating scenarios, i.e., for all PRF's, antenna speeds, etc.

Conclusions and Recommendations

Doppler radars (i.e., coherent radars) equipped with dual polarization have the capabiality to measure the full covarience matrix of co-polar and cross-polar echoes.

These measurements can be made with either dual linear, i.e., horizontal and vertical polarization, or with dual circular, i.e., right and left hand circular. The meteorological information produces different signal characteristics for the linear and circular polarization and thus different signal analyses are done. The overall computational complexity is greater for dual circular. (Also the radar antenna sidelobe requirements are more stringent

for circular). The technique recommended for consideration by NEXRAD is dual linear polarization.

The three measurements of prime interest in the meteorological application are: (1) Differential reflectivity defined as the ratio of reflectivities at orthogonal polarizations. The two reflectivities are different if the hydrometeors are anisotropic and have a preferred orientation, (2) Differential propagation constant defined as the rate of change of the difference between the phase of horizontal and vertical polarization. This parameter is different for isotropic and anisotropic scatterers (such as hailstones and raindrops), (3) Correlation coefficient between orthogonal polarizations. This parameter is sensitive to orientation and shape of the hydrometeors.

The combination of these three parameters provides significant system enhancements over single polarization in: a) reduction of rainfall rate estimate variance (no significant improvement in mean estimate except at higher rates, however); b) distinguishing scatter phase state; and c) capability to categorize hail size.

Theoretically, it has been shown that useful measurements of these parameters can be made without impact on the system prime mission. The differential measurements require a different waveform but the Doppler measurements can be adapted to this waveform without compromising velocity moment estimate variance or radar antenna scan rate.

Engineering changes for the dual polarization measurements can be grouped into the following three general areas, microwave, signal processing, and data analysis. Hardware changes (for dual linear) at the microwave level, consist of the addition of a fast switch, an orthomode coupler, and scaler feed (the existing NEXRAD circular feed may be suitable as is). The signal processing changes are hardware-firmware and consist of adapting the existing

reflectivity, velocity and spectrum width calculators for operation with the dual polarization waveform and the addition of calculations for differential reflectivity and differential phase. The differential phase and reflectivity calculation are very similar in complexity to the existing velocity calculations. The data analysis changes are software modifications to incorporate the measurements into output products. It is anticipated that these changes can be easily absorbed by the existing system.

Full scale modification of NEXRAD for dual polarization is not recommended at this time. We have estabalished the operational potential of dual polarization and the compatibility of the measurement with the prime mission of the radar. However, the utility and cost effectiveness of the technique for the operational agencies has yet to be demonstrated. We recommend that a pseudo-operational system be configured and program established to demonstrate the technique and provide data for evaluation.

References

Aydin, K., T.A. Seliga, and V. Balaji, 1986: "Remote sensing of hail with a dual linear polarization radar", J. Clim. Appl. Meteorol., 25, pp. 1475-1484.

Balakrishnan, N., D.S. Zrnic', J. Goldhirsh, and J. Rowland, 1988a: "Comparison of simulated rain rate accuracies from disdrometer data employing polarimetric radar algorithms". Submitted to J. Atmos. Oceanic Tech.

Balakrishnan, N., and D.S. Zrnic', 1988b: "Quantification of rain and hail in a mixture from polarimetric measurements," to be submitted, J. Atmos. Sci.

Battan, L.J., 1973: Radar Observations of the Atmosphere, University of Chicago Press, Chicago, Illinois, 324 pp.

Bringi, V.N., R.M. Rasmussen, and J. Vivekanandan, 1986: "Multiparameter radar measurements in Colorado convective storms Part I: Graupel melting studies", J. Atmos. Sci., Vol. 43, No. 22, Nov., pp. 2545-2563.

Bringi, V.N., T.A. Seliga, and K. Aydin, 1984: "Hail detection with a differential reflectivity radar", Science, 225, pp. 1145-1157.

Bringi, V.N., T.A. Seliga, and S.M. Cherry, 1983: "Statistical properties of the dual polarization differential reflectivity (Z_{DR}) radar signal", IEEE Trans. Geosci. Remote Sens., GE-21, pp. 215-220.

Carter, J.K., D. Sirmans, and J. Schmidt, 1986: "Engineering description of the NSSL dual linear polarization Doppler weather radar", Preprint, 23rd Conference on Radar Meteorology, AMS, Snowmass, Colorado, pp.

Cheng, L., and M. English, 1983: "A relationship between hailstone concentration and size", J. Atmos. Sci., 40, pp. 204-213.

Doviak, R.J. and D.S. Zrnic', 1984: **Doppler Radar and Weather Observations,** Academic Press, 458 pp.

Goddard, J.W.F., and S.M. Cherry, 1984: "The ability of dual polarization radar (co-polar linear) to predict rainfall rate and microwave attenuation", Radio Science, 19, pp. 201-208.

Goldhirsh, J., J. Rowland, and B. Musiani, 1987: "Rain measurement results derived from a two-polarization frequency-diversity S-band radar at Wallops Island, Virginia", IEEE Trans. Geosic. Remote Sens., GE-25, pp. 654-661.

Illingworth, A.J., J.W.F. Goddard, and S.M. Cherry, 1987: "Polarization radar studies of precipitation development in convective storms", Qtr. J. Roy. Meteor. Soc., 113, pp. 469-489.

Knight, C.A., and N.C. Knight, 1970: "The falling behavior of hailstones, J. Atmos. Sci, 27, pp. 672-681.

Leitao, M.J., and P.A. Watson, 1984: "Application of dual-linearly polarized radar data to prediction of microwave path attenuation at 10-30 GHz", Radio Science, 19, pp. 209-221.

Lipshutz, R.C., J.F. Pratte, and J.R. Smart, 1986: "An operational Z_{DR}-based precipitation type/intensity product", Preprint, 23rd Conf. on Radar Meteorology, AMS, Snowmass, Colorado, pp. JP91-JP94.

List, R., 1983: "Properties and growth of hailstones" in **Thunderstorms Morphology and Dynamics**, E. Kessler (Ed.), University of Oklahoma Press, Norman, Oklahoma, pp. 259-276.

Longtin, D.R. et al. 1987: "Radar back scattering by large, oblate spongy ice spheroids", J. Atmos. Oceanic Tech., 4, pp. 355-358.

Metcalf, J.I., and G.M. Armstrong, 1983: "A polarization diversity radar data processor", Preprint, 21st Conf. on Radar Meteorology, AMS, Edmonton, Alberta, Canada, pp. 339-345.

Mueller, E.A., and D.W. Staggs, 1986: "Capabilities of the CHILL radar after update", Preprints, 23rd Conf. on Radar Meteorology, Snowmass, Colorado, AMS, pp. JP352-JP353.

Mueller, E.A., 1984: "Calculation procedure for differential propagation phase shift", Preprint, 22nd Conf. on Radar Meteorology, AMS, Zurich, Switzerland, pp. 397-399.

Oguchi, T., 1983: "Electromagnetic propagation and scattering in rain and other hydrometeors", Proc IEEE, 71, 1029-1078.

Sachidananda, M., and D.S. Zrnic', 1985: "Z_{DR} measurement consideration for a fast scan capability radar", Radio Science, 20, pp. 907-922.

Sachidananda, M., and D.S. Zrnic', 1986: "Differential propagation phase shift and rainfall rate estimation", Radio Science, 21, pp. 235-347.

Sachidananda, M., and D.S. Zrnic', 1987: "Rain rate estimates from differential polarization measurements", J. Atmos. and Ocean. Tech., 4, pp. 588-598.

Sachidananda, M., and D.S. Zrnic', 1988: "Efficient processing of alternately polarized radar signals". Submitted to J. Atmos. and Oceanic Tech.

Schnabl, G., M. Chandra, A. Schroth, and E. Lüneburg, 1986: "The advanced polarimetric DFVLR radar: First measurements and its unique signal-processing and calibration aspects", Preprint, 23rd Conf. on Radar Meteorology, AMS, Snowmass, Colorado, pp. 159-164.

Seliga, T.A., and V.N. Bringi, 1976: "Potential use of radar differential reflectivity measurements at orthogonal polarizations for measuring precipitation", J. Appl. Meteorol., 15, pp. 69-76.

Seliga, T.A., and V.N. Bringi, 1978: "Differential reflectivity and differential phase shift: Applications in radar meteorology", Radio Science, 13, pp. 271-275.

Sirmans, D., D. Zrnic', and M. Sachidananda, 1986: "Doppler radar dual polarization-consideration for NEXRAD", Internal Report for JSPO.

Sirmans, D., and J.T. Dooley, 1986: "A numerical comparison of three differential reflectivity estimates", Preprints, 23rd Conference on Radar Meteorology, AMS, Snowmass, Colorado, pp.

Steinhorn, I., and D.S. Zrnic', 1988: "Potential uses of differential propagation phase constant to estimate raindrop and hailstone size distributions", IEEE Trans Geosci. Remote Sens., September, IGARSS '87, Special Issue.

Ulbrich, C.W., and D. Atlas, 1984: "Assessment of the contribution of differential polarization to improved rainfall measurements", Radio Sci., 19, pp. 49-57.

Waldvogel, A., B. Federer, and P. Grimm, 1979: "Criteria for detection of hail cells", J Appl. Meteorol., 18, pp. 1521-1525.

Zrnic', D.S., 1977: "Spectral moment estimates from correlated pulse pairs", IEEE Trans. Aerosp. Elect. Sys., AES-13, pp. 344-354.

Zrnic', D.S., 1979: "Estimation of spectral moments for weather echoes", IEEE Trans. Geosic. Remote Sens., GE-17, pp. 113-128.

Zrnic', D.S., N. Balakrishnan, and M. Sachidananda, 1988: "Processing and interpretation of alternately polarized weather radar echoes", Preprints, IGARSS '88.

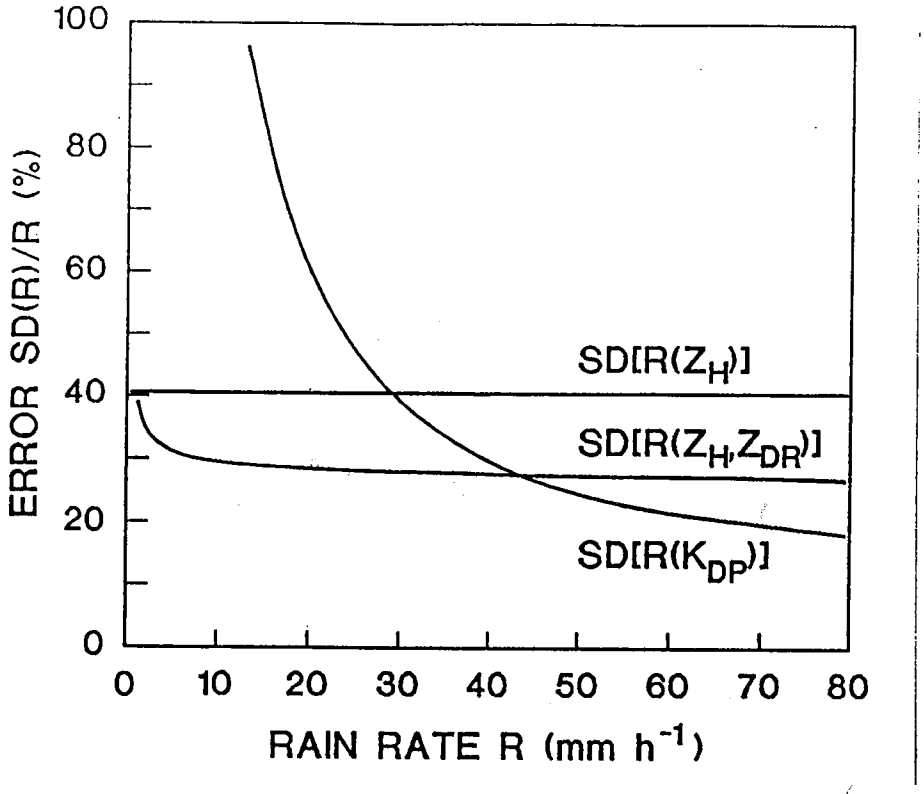

Figure 1.1 Normalized standard errors of rain rate estimates for three estimators. Errors account for statistical uncertainty of the estimates and variations in the drop size distribution.

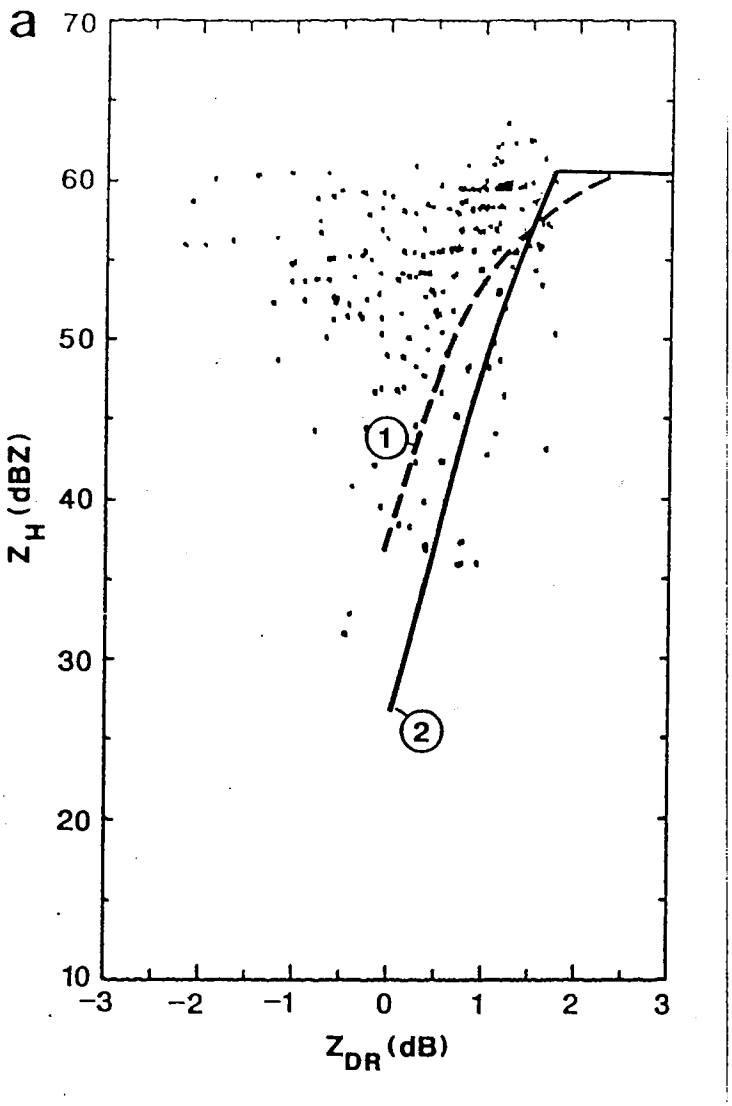

Figure 1.2 Scatterogram of Z_H, Z_{DR} data from a hailstorm; Boundary 1 between rain and hail is from Leitao and Watson (1984) and boundary 2 from Aydin et al. (1986)

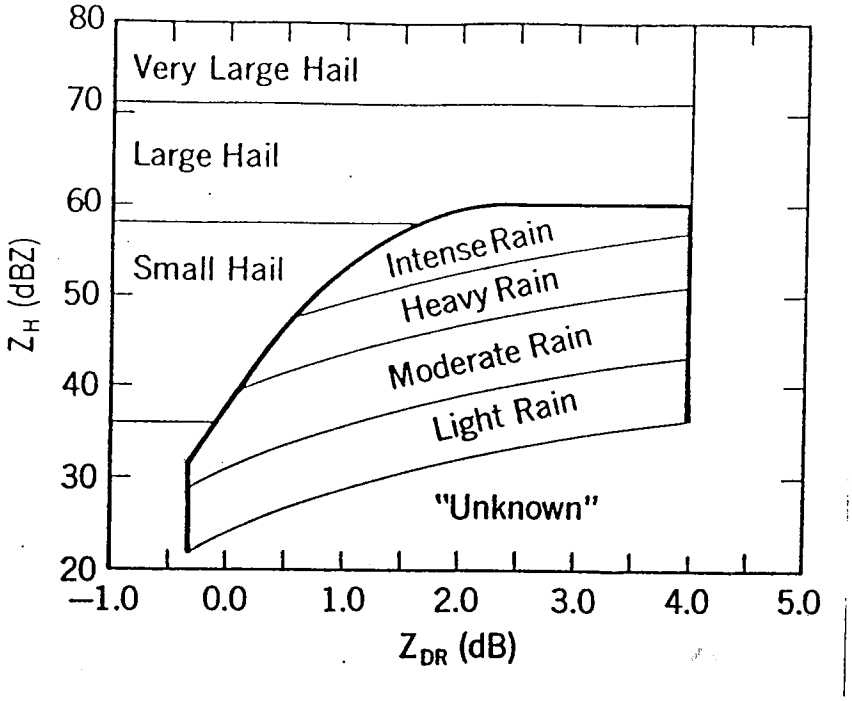

Figure 1.3 (a) The precipitation type/intensity model from Lipshutz et al. (1986). Bold line is rain/hail boundary given by Leitao and Watson (1984).

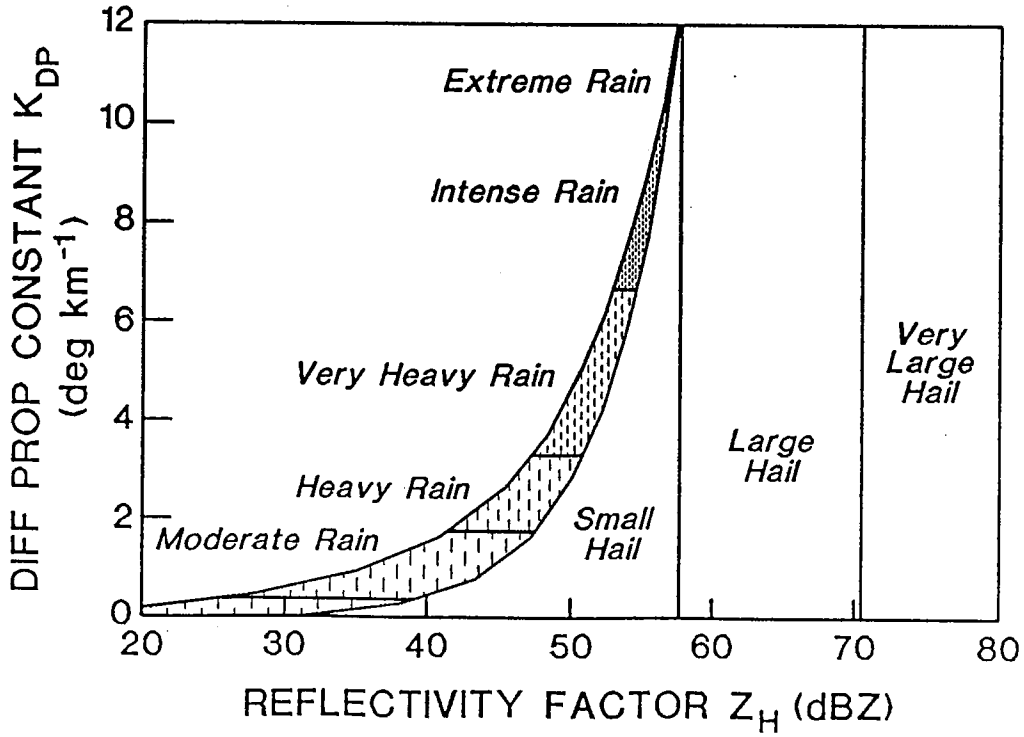

(b) The precipitation type/intensity model in the K_{DP}-Z_{DR} planes corresponding to the model in (a).

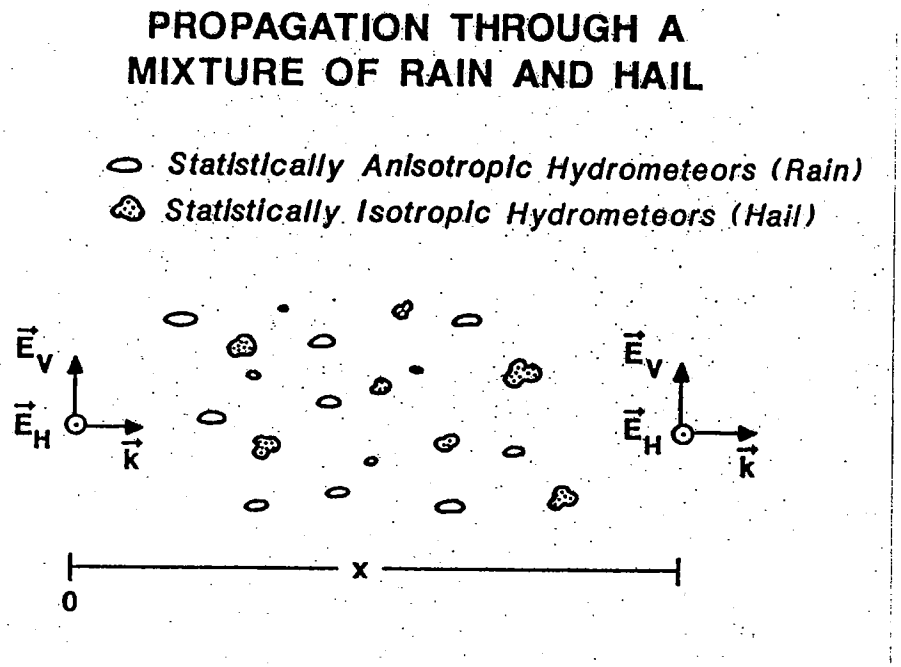

Figure 1.4 Propagation through a mixture of rain and hail.

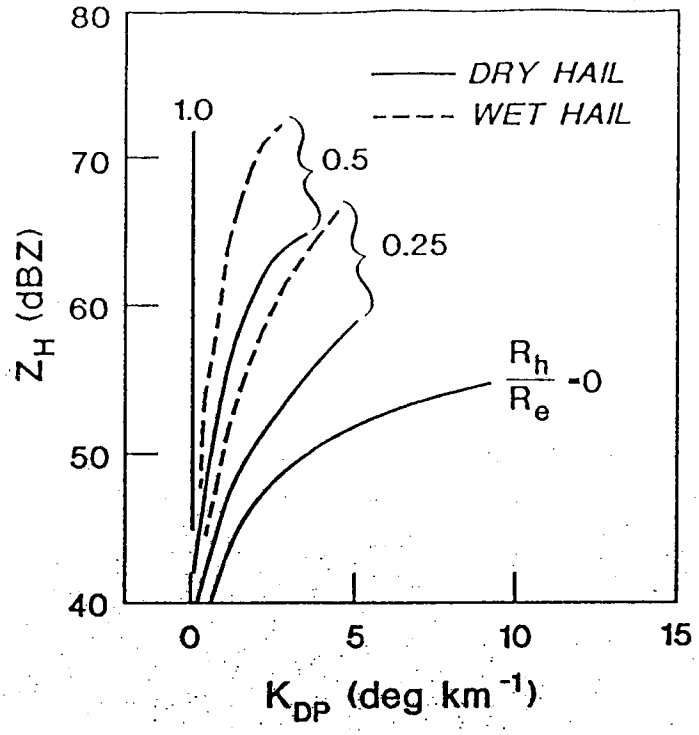

Figure 1.5 (a) Z_H-K_{DP} curves for fixed proportions of hail and rain in a mixture. R_h is hail rate and R_e is the equivalent total rain plus hail rate. Hailstones are assumed to be spherical, obey Cheng-English distribution and are either dry or very wet (i.e., dielectric constant of water).

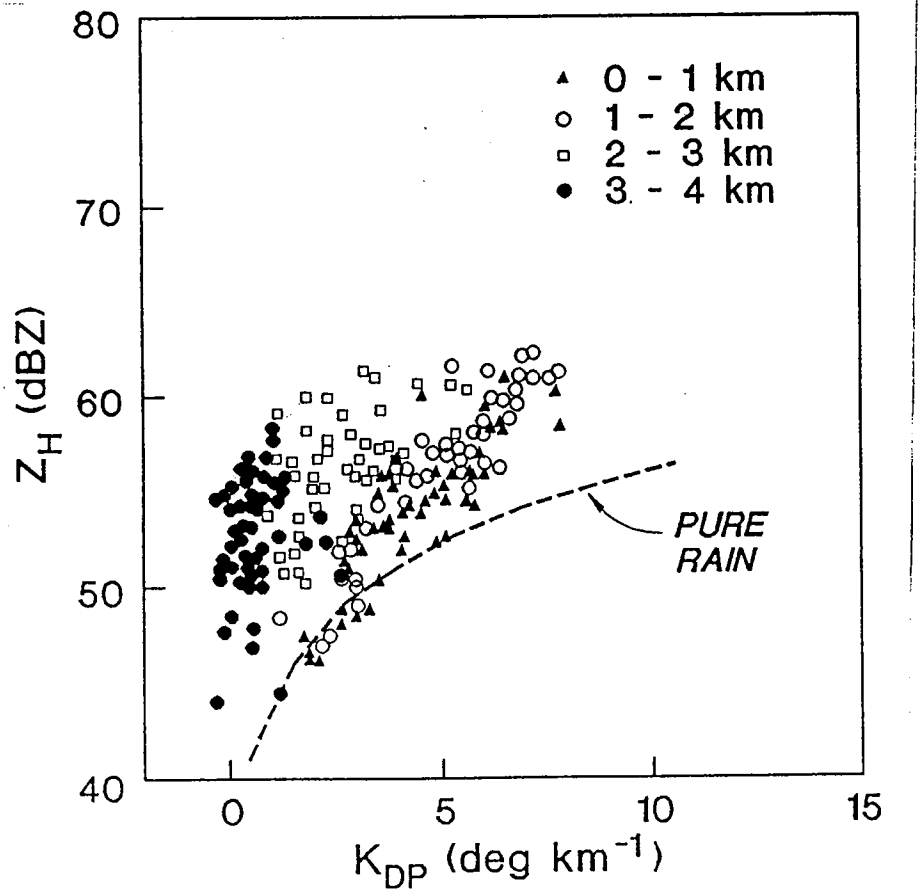

(b) Data of Z_H, K_{DP} pairs stratified by height and from a storm that produced rain and hail on the ground.

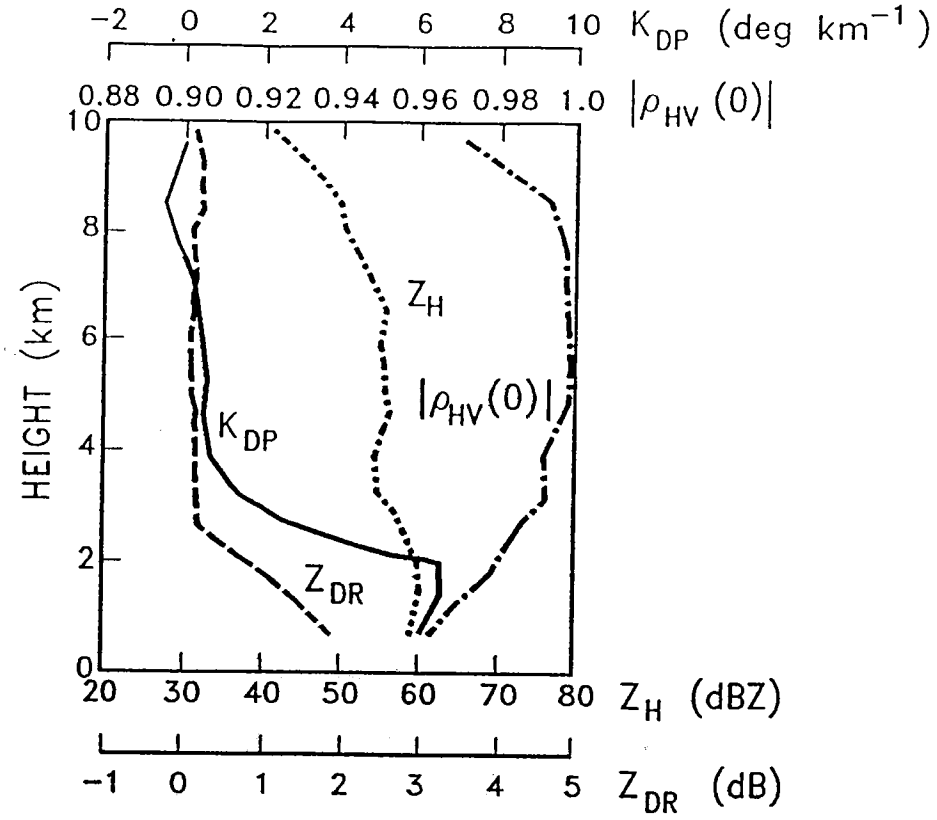

Figure 1.6 (a) Vertical profiles of Z_H, Z_{DR}, K_{DP} and $|\rho_{HV}(o)|$ on May 14, 1986 at 15:59:32 CST range of 40 km, and azimauth of 130°.

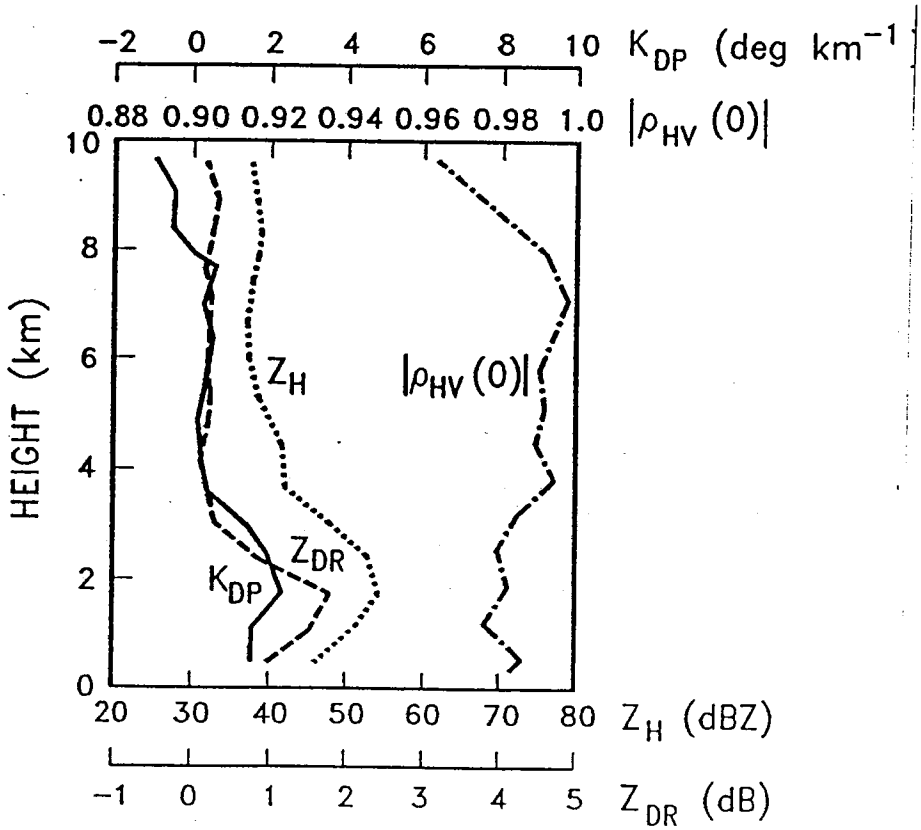

(b) Same as (a) but at 16:11:06 CST. The estimates represent averages over 2.4 km in range.

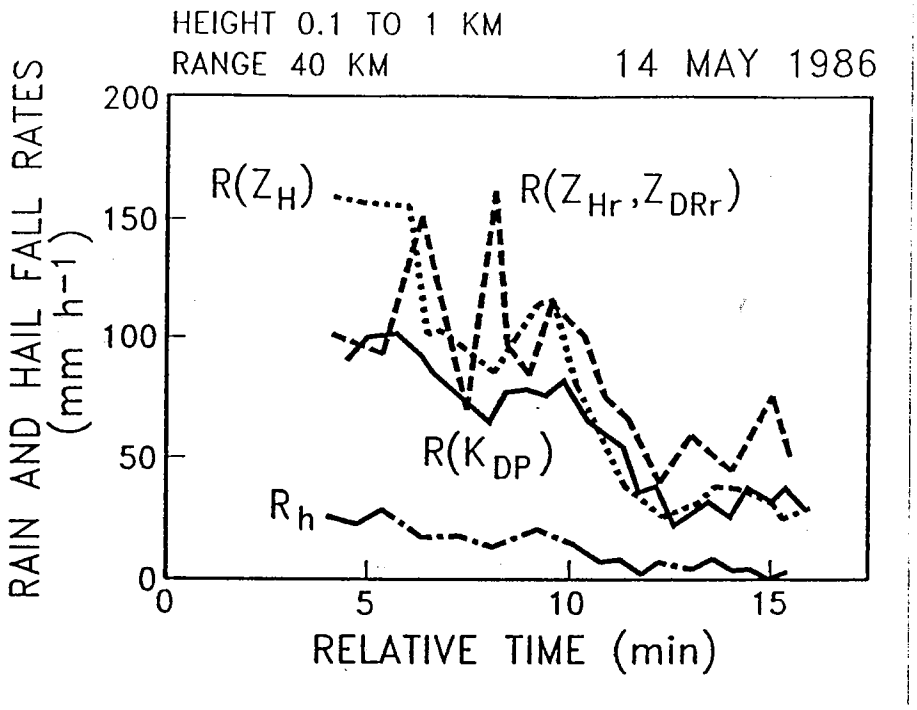

Figure 1.7 Rain and hail rates versus relative time with respect to 15:55:00 CST.

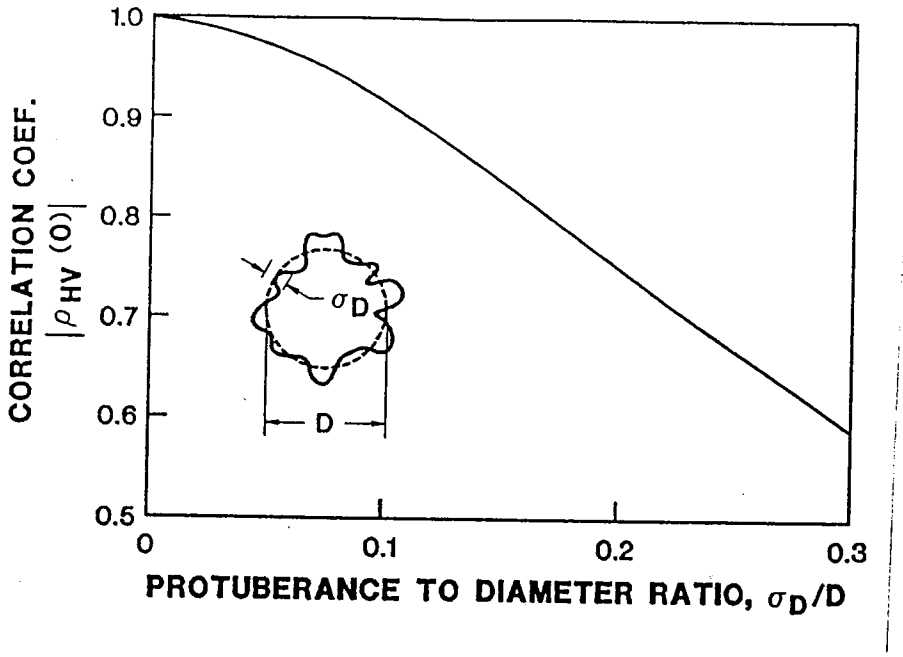

Figure 1.8 Dependence of the correlation coefficient on the protuberance to diameter ratio. Rayleigh scattering is assumed and the diameter is for a sphere with volume equal to an irregular hailstone.

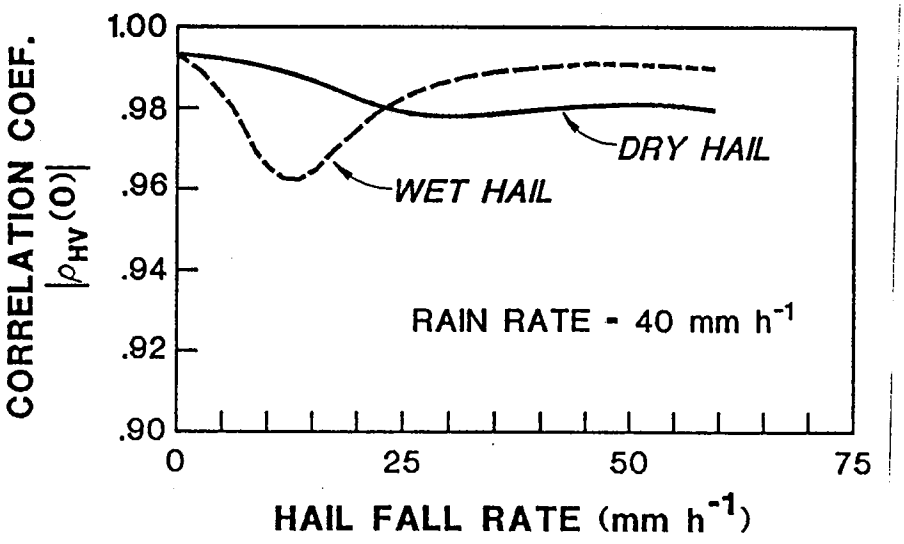

Figure 1.9 Correlation coefficient for a mixture of rain and hail. A fixed rain rate is 40 mm h^{-1}. Hailstones are modeled as oblate spheroids with axis ratio of 0.8, and the minor axis is oriented horizontally. Size distribution is exponential as given by Cheng and English (1983).

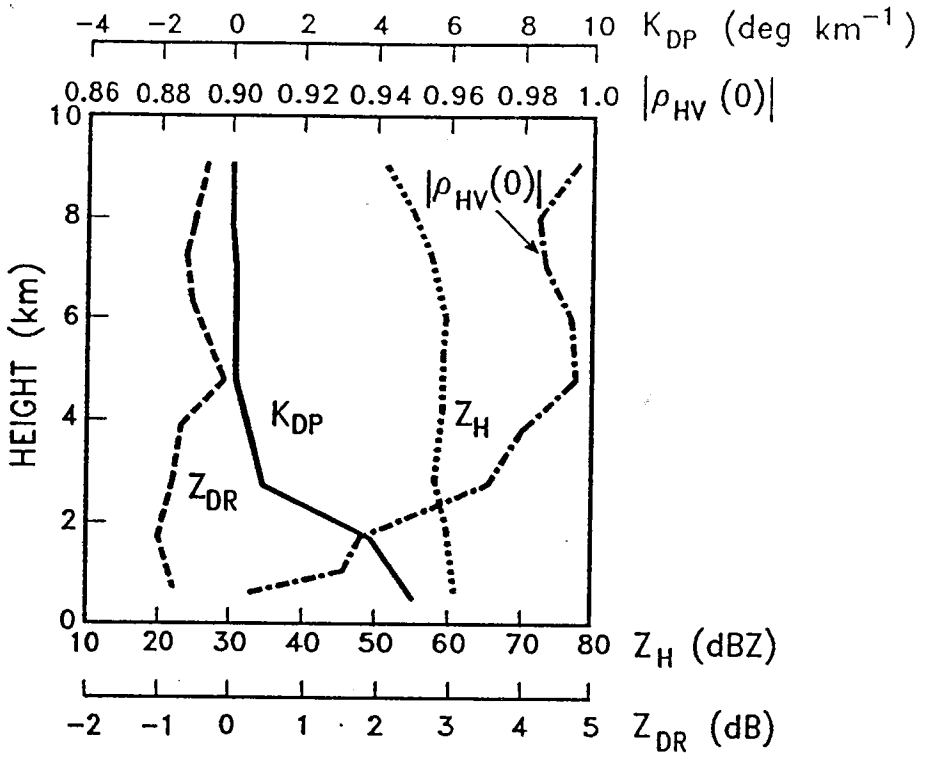

Figure 1.10 Vertical profiles of Z_H, Z_{DR}, K_{DP} and $|\rho_{HV}(o)|$ on June 2, 1985 at 18:59:28 CST, range of 82.5 km, and azimuth of 242°. The estimates represent averages over 2.4 km in range.

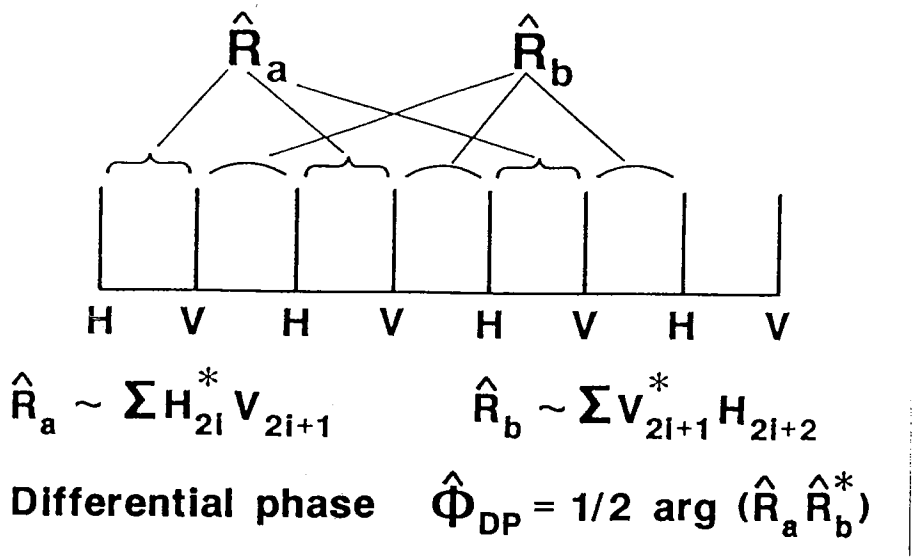

Figure 2.1 A sequence of alternately polarized echoes, horizontal H and vertical V. Two autocovariance estimates that show simultaneous retrieval of Doppler and differential phase are indicated.

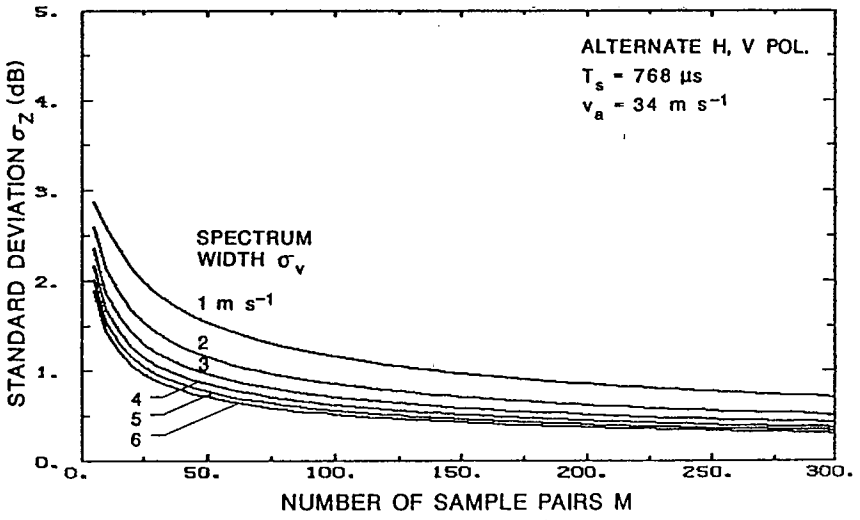

Figure 2.2 Standard error of Z_H estimates. Because this graph is for alternate samples, the number of sample pairs equals to the number of reflectivity samples at horizontal or vertical polarization.

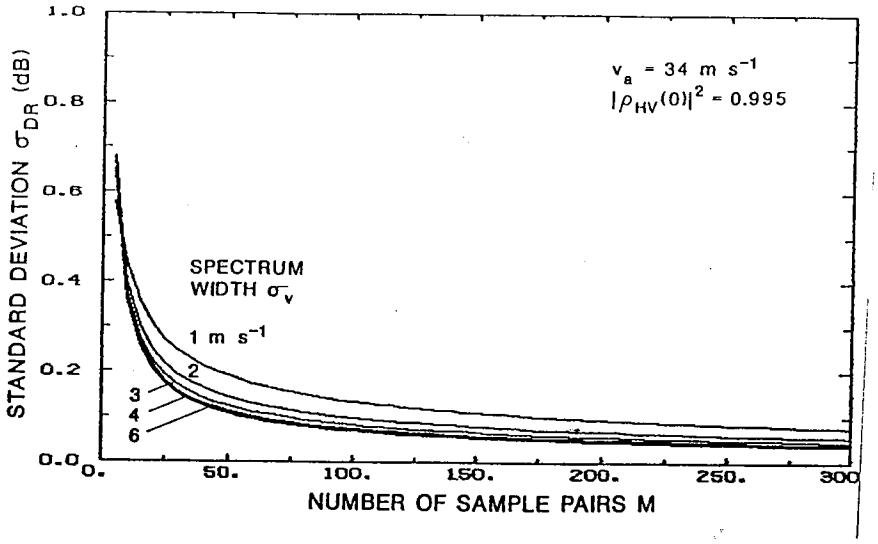

Figure 2.3 Standard error of Z_{DR} estimates. $\rho_{HV}(0)$ is the correlation coefficient between echoes at horizontal and vertical polarization at lag 0. (Sachidananda and Zrnic', 1985).

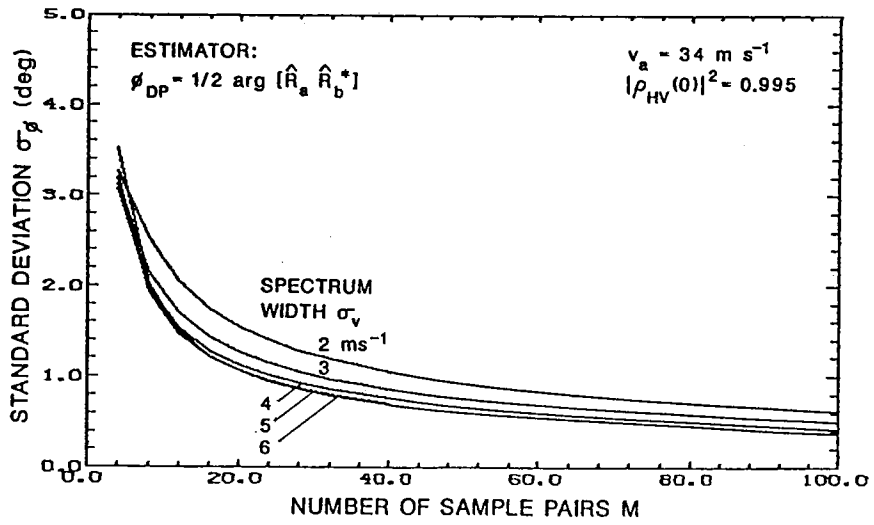

Figure 2.4 Standard error in ϕ_{DP} estimates. $\rho_{HV}(0)$ is the correlation coefficient between horizontally and vertically polarized echoes at lag 0.

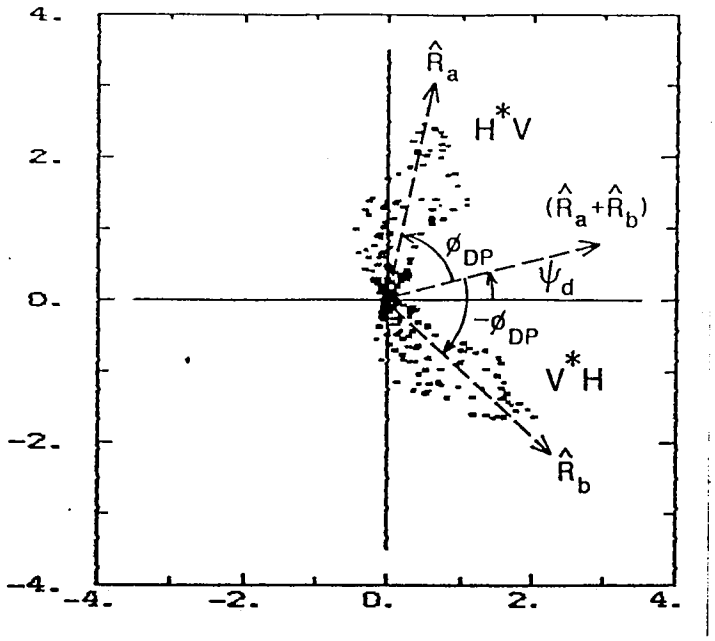

Figure 2.5 Complex pulse pair product vectors from a time series record. x,y axes are in arbitrary units.

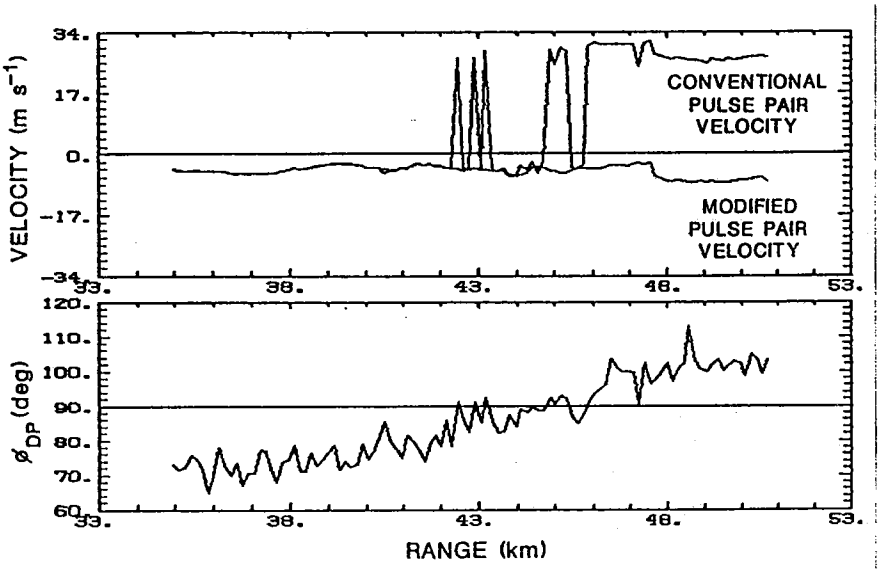

Figure 2.6 A comparison of velocity estimates from the conventional pulse pair estimator (2.4) and the modified estimator (2.15). The corresponding ϕ_{DP} estimates are also shown. Discrete data are spaced in range by 150 m, but are connected for visual clarity.

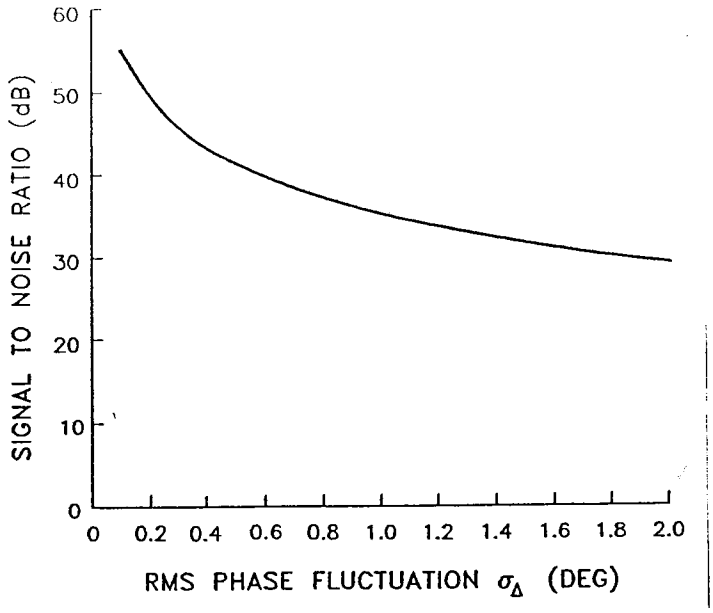

Figure 2.7 Equivalent signal-to-noise ratio produced by random phase fluctuations.

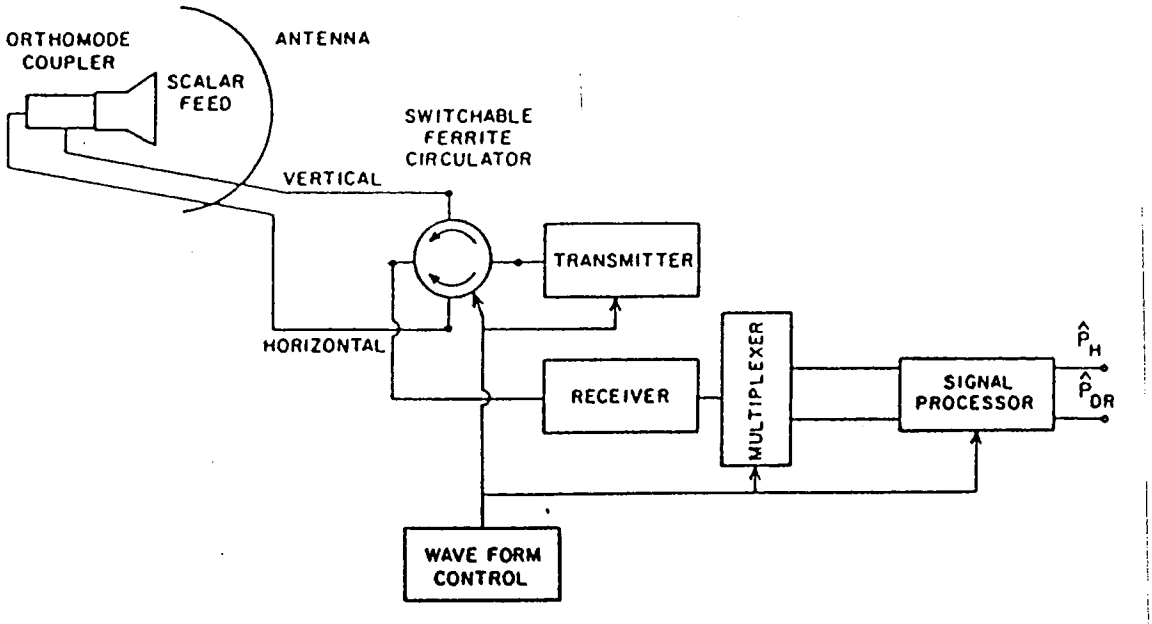

Figure 3.1 Block diagram of NEXRAD configured for dual polarization capability.

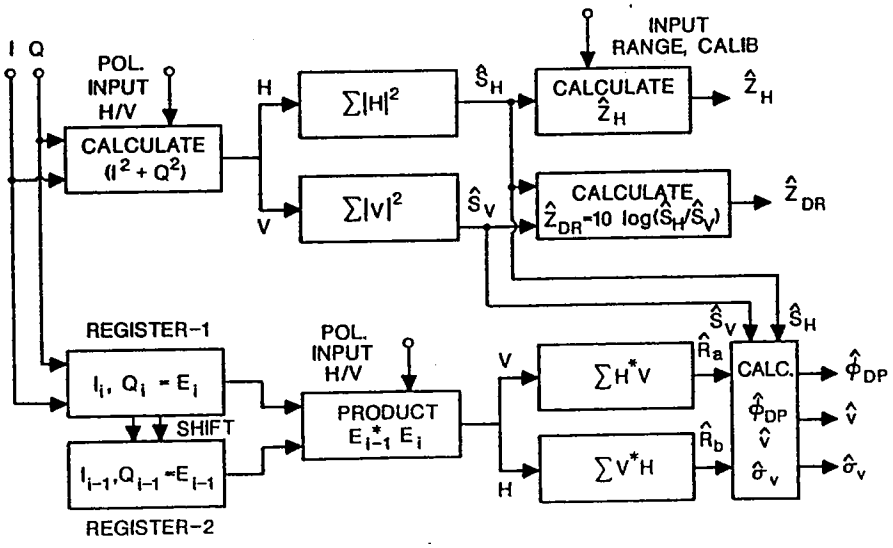

Figure 3.2 A signal processing scheme for dual polarization measurements.

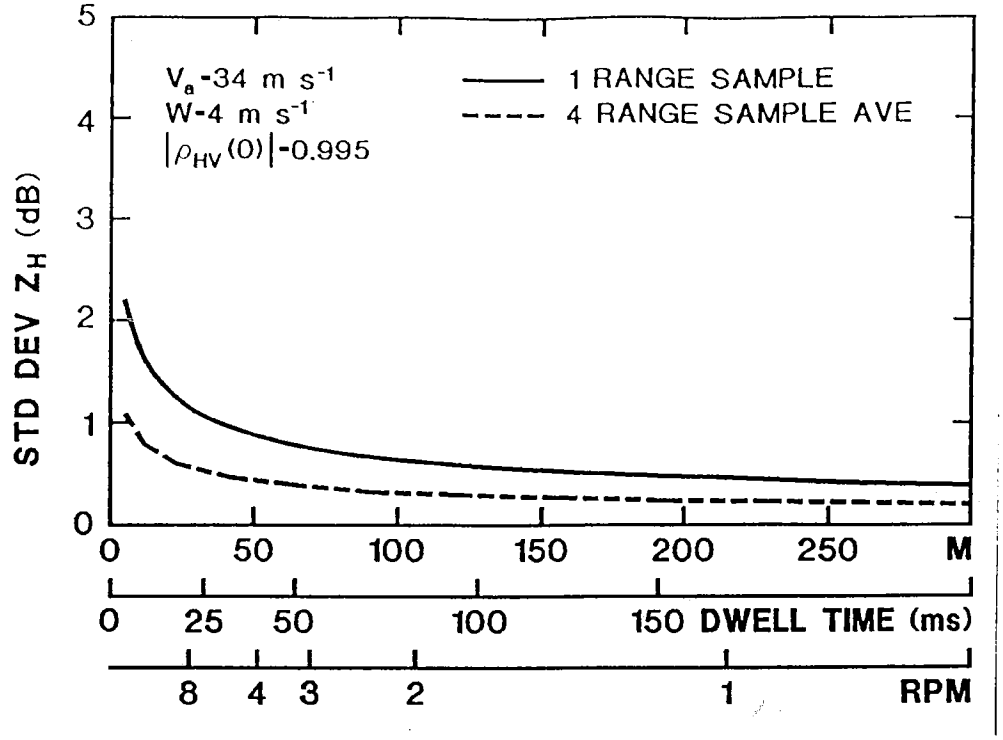

Figure 3.3 Standard deviation of horizontal reflectivity estimate related to radial dwell time and antenna rotation rate for radials spaced by 1° in azimuth.

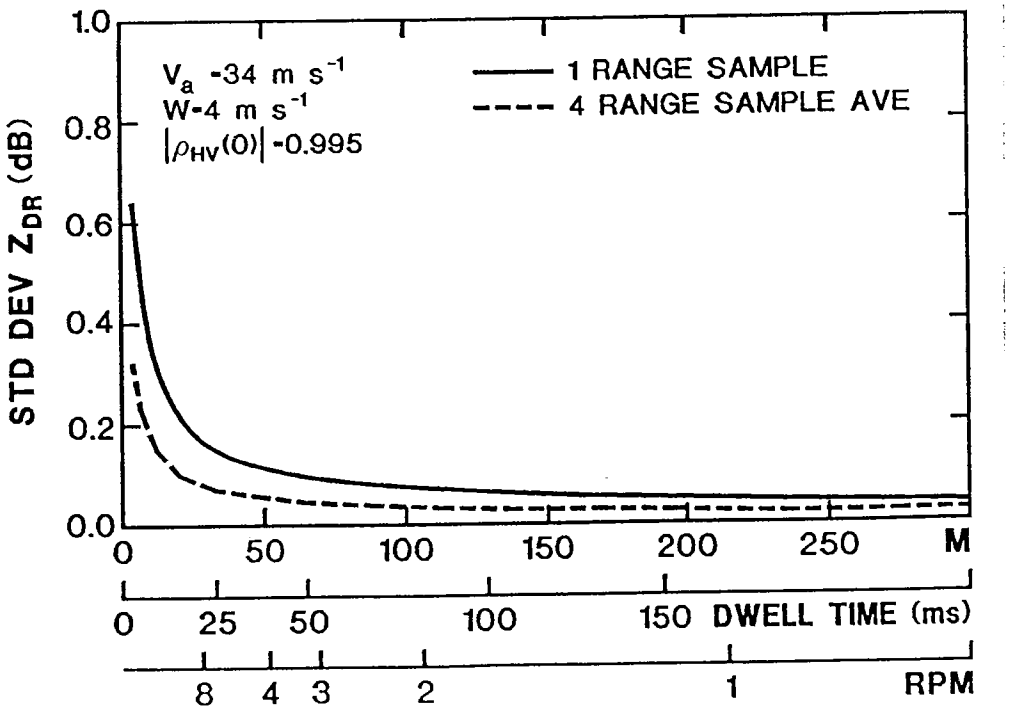

Figure 3.4 Standard deviation of differential reflectivity estimate related to radial dwell time and antenna rotation rate for radials spaced by 1° in azimuth.

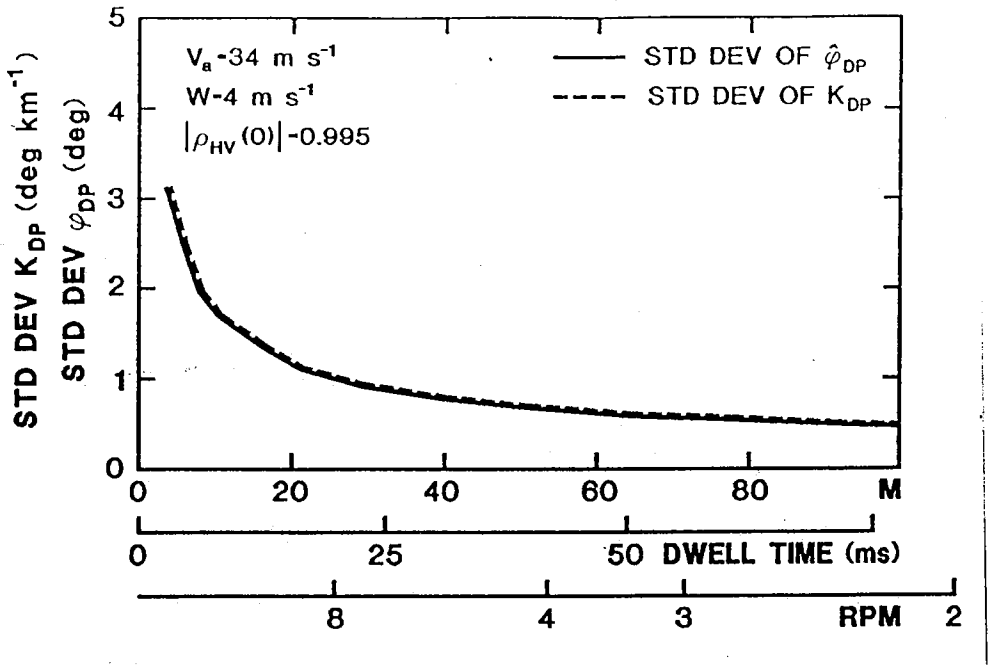

Figure 3.5 Standard deviation of differential phase and phase gradient related to radial dwell time and antenna rotation rate for radials spaced by 1° in azimuth.